REMARKS

Applicants respectfully request reconsideration of the present application in view of the foregoing amendments and in view of the reasons that follow.

Claims 2 and 6-8 are requested to be cancelled as they are now incorporated into claim 1. Claims 1, 3-5 and 9 are currently being amended to incorporate the limitations of the canceled claims and correct claim dependencies. Support for this amendment can be found, *inter alia*, in the Examples and Figures 3 and 4 of the specification.

This amendment adds, changes and/or deletes claims in this application. A detailed listing of all claims that are, or were, in the application, irrespective of whether the claim(s) remain under examination in the application, is presented, with an appropriate defined status identifier.

After amending the claims as set forth above, claims 1, 3-5 and 9 are now pending in this application.

Interview with Examiner Leavitt

Applicants thank Examiner Leavitt for her helpful discussion with Applicants' representative, Victoria Statham (formerly Rutherford) on May 27, 2008, clarifying several issues regarding the Office Action as discussed below.

Information Disclosure Statement

The Examiner has indicated that the following references have not been considered for failure to provide a legible copy. While Applicants assert that such copies were submitted with the Information Disclosure Statement filed April 7, 2005, copies of these documents are resubmitted for the Examiner's convenience and consideration.

A1 Japanese Pat. App. No. 2000-139470

A2 Japanese Pat. App. No. 2001-161384

A4 Tanaka et al., *Biochemical and Biophysical Research Communications* (2001) 286:547-553.

A5 Tanaka et al., *Cancer Gene Therapy* (2002) 9:483-488.

Objections to the Drawings

The Examiner has objected to the Figures 3A-D and 4A-D for being too dark. Upon further discussion in the teleconference with Applicants' representative, it was discovered that the color photographs that were filed on April 7, 2005 with the appropriate Petition and fee, were not properly entered into the Patent Office records nor routed to the Examiner. As such, these color photographs filed herewith are a resubmission of the originally filed figures, not amendments. Entry and consideration are respectfully requested.

Claim Rejections

Rejections under 35 U.S.C. § 101 – Utility

Claims 1-9 were rejected under 35 U.S.C. § 101 for allegedly lacking a specific and substantial utility or a well-established utility. Applicants respectfully traverse this rejection.

The claims are directed to a chimeric mouse containing a disrupted endogenous Bradeion gene, with a chimeric rate from 90% to 98%, and exhibits malformation which is at least one selected from the group consisting of cranial dysplasia, visual disorders, and generalized decreased growth compared with those of the same strain without the disrupted Bradeion gene. Thus, the claimed mouse has a specific genotype (disrupted Bradeion gene), phenotype (cranial dysplasia, visual disorders, and generalized decreased growth) and a high degree of chimerism.

The Examiner asserts that the disruption of the Bradeion gene is not associated with the claimed pheontype. Specifically, the Examiner states

> [t]he specification does not teach any examples of chimeric heterozygous and/or homozygous mice associating the disruption of the Bradeion gene with any cranial dysplasia, visual disorders, and generalized decreased growth.

Office Action, page 7 (emphasis in the original). The Examiner goes on to note that the instant chimeric mouse is shown to have this phenotype in Figures 3 and 4, but goes on to state that "the claimed pheotypes may be associated with disruption of other genes in addition to Bradeion." Office Action, page 8. Furthermore, the Examiner states that because Bradeion gene expression is implicated in some cancers, that the claimed phenotype is unexpected and that one of skill would not find utility in the absence of teaching the role of Bradeion gene in the claimed phenotype. Applicants respectfully disagree.

To fulfill the utility requirements of 35 U.S.C. § 101, the claimed invention must have a specific and substantial utility. *See* MPEP 2707.01. Furthermore, the asserted utility must be credible. As discussed in MPEP § 2107.03, "evidence of pharmacological or other biological activity of a compound will be relevant to an asserted therapeutic use if there is a reasonable correlation between the activity in question and the asserted utility. "*Cross v. Iizuka*, 753 F.2d 1040, 224 USPQ 739 (Fed. Cir. 1985); *In re Jolles*, 628 F.2d 1322, 206 USPQ 885 (CCPA 1980); *Nelson v. Bowler*, 626 F.2d 853, 206 USPQ 881 (CCPA 1980). Applicants assert that this requirement has been met.

The present specification discloses, among others, the usefulness of using the claimed mice in the study of abnormalities in the central nervous system. Page 19, lines 25-29; see also page 4, lines 4-9. Further, the specification discloses that Bradeion is associated with the long-term survival of human cerebral neurons after differentiation (page 4, line 23 through page 5, line 9) and that expression of the human Bradeion gene is found in human adult cerebral nerve system cells, further stating that Bradeion is a potential target for diagnosis and gene therapy for cell mutations (page 2, lines 4-10). Indeed, as briefly noted by the Examiner on page 9 of the Office Action, Tanaka et al. (*Biochem. Biophys. Res. Comm.* (2001) 286:547-553; Reference A4 of the Information Disclosure Statement filed April 7, 2005)

underscores the importance of Bradeion gene expression in the human central nervous system by showing data indicating its expression in the brain. A person of skill in the art would even expect the correlation of Bradeion gene expression in cancer given its known function as a cell division factor, a process known to be disrupted in cancer. Therefore, while the exact molecular mechanism for the function of Bradeion is not yet known, there is a strong correlation between Bradeion and the central nervous system, as evidenced by gene expression studies in the art as well as the phenotype exhibited by the claimed mice.

In further support for the usefulness of the claimed chimeric mice in the study of cerebral abnormalities, Exhibit A (Ihara *et al. J. Biol. Chem.* (2003) 278:24095-24102) shows the association of a protein of the septin family, of which Bradeion is also a member, with Parkinson's disease. Likewise, Exhibit B (Kinoshita *et al. Am. J. Pathol.* (1998) 153:1551-1559) shows the association of septin proteins in Alzheimer's disease. Without being limited to these findings, it is reasonable, based on the similarity of the Bradeion gene (a septin) with the septins associated with the human neurological disorders as well as the observed phenotype of the mice, to believe that these mice may be useful for the study of these human disorders.

The Examiner should not be confused by the fact that the chimeric mouse may itself be used in further research, as MPEP § 2107.01 confirms that many such "research tools" have a "clear, specific and unquestionable utility", albeit in the research setting. Here, there is no further research needed to identify the utility of the claimed chimeric mouse, as there is a reasonable correlation between the disruption of the Bradeion gene in these mice and the displayed phenotype as being useful for studying central nervous system abnormalities.

With regards to the Examiner's assertion that the phenotype may be due to the disruption of genes other than Bradeion, Applicants respectfully assert that this allegation is unreasonable. First, as discussed, the specification provides a clear link between Bradeion gene and the brain, such that the phenotype observed is quite reasonably associated with the disruption of the gene. Second, the art has long recognized the specificity of gene knockouts. As shown in the attached Exhibit C (Thomas and Capecchi, *Nature* (1990) 346:847-850), gene targeting vectors are designed based on sequence homology to target a particular gene

and remove it. The nonspecific vector elements, such as the reporter gene, have been repeatedly used in different targeting vectors used in standard techniques used by those skilled in the art with minimal or no impact. Indeed, the Nobel Prize was recently awarded to one of the authors of Exhibit C, Mario Capecchi, for his work in developing this knockout technology, illustrating the widespread recognition and acceptance of mouse knockout technology.

Based on the reasonable correlation between the disruption of the Bradeion gene, the phenotype of the chimeric mice and the known association with the Bradeion gene in particular as well as septin proteins in general with disorders of the central nervous system, Applicants assert that the claimed chimeric mouse has a specific, substantial and credible utility. Therefore, Applicants respectfully request that the rejection be withdrawn.

Rejections under 35 U.S.C. § 112, First paragraph - Enablement

Claims 1-9 were rejected under 35 U.S.C. § 112, first paragraph for allegedly lacking enablement by the specification. Applicants respectully traverse this rejection.

Specifically, the Examiner questions the scope of the claims, stating that they are generically drawn to a transgenic mouse in which the Bradeion is suppressed. The Examiner asserts that the claims encompass a mouse with any level of Bradeion suppression and any phenotype, a concern reiterated in the Interview of May 27, 2008.

The test of enablement is whether one reasonably skilled in the art could make or use the invention from the disclosures in the patent coupled with information known in the art without undue experimentation. *United States v. Telectronics, Inc.,* 857 F.2d 778, 785, 8 USPQ2d 1217, 1223 (Fed. Cir. 1988) See also MPEP § 2164.01. First, the scope of the claims must be examined. Without acquiescing to the rejection, the claims have been amended to recite that the Bradeion be disrupted, rather than suppressed as recited previously. Further the mouse must have a chimeric rate of between 90-98%, as supported by the Examples in the specification, and that the phenotype of the mice include cranial dysplasia,

visual disorders and hypoplasia as compared to the normal mouse, all of which have actually been observed in the chimeric mice, as discussed in the Examples and shown in Figures 3 and 4. Indeed, these characteristics have been observed in multiple chimeric mice generated from at least two different embryonic cell lines, indicating that the scope of the present claims are well supported by the teachings of the specification.

As the methods disclosed in the specification can reliably be used to generate chimeric mice within the scope of the present claims, Applicants respectfully assert that one of skill in the art have ample guidance on how to make and use the present invention. Therefore, Applicants respectfully request that the rejection be withdrawn.

CONCLUSION

Applicants believe that the present application is now in condition for allowance. Favorable reconsideration of the application as amended is respectfully requested.

The Examiner is invited to contact the undersigned by telephone if it is felt that a telephone interview would advance the prosecution of the present application.

The Commissioner is hereby authorized to charge any additional fees which may be required regarding this application under 37 C.F.R. §§ 1.16-1.17, or credit any overpayment, to Deposit Account No. 19-0741. Should no proper payment be enclosed herewith, as by a check being in the wrong amount, unsigned, post-dated, otherwise improper or informal or even entirely missing or a credit card payment form being unsigned, providing incorrect information resulting in a rejected credit card transaction, or even entirely missing, the Commissioner is authorized to charge the unpaid amount to Deposit Account No. 19-0741.

If any extensions of time are needed for timely acceptance of papers submitted herewith, Applicants hereby petition for such extension under 37 C.F.R. §1.136 and authorizes payment of any such extensions fees to Deposit Account No. 19-0741.

Respectfully submitted,

Date June 6, 2008

By Victoria S. Ruthford
for Reg # 52,253

FOLEY & LARDNER LLP
Customer Number: 22428
Telephone: (202) 672-5404
Facsimile: (202) 672-5399

Stephen A. Bent
Attorney for Applicants
Registration No. 29,768

EXHIBIT A

THE JOURNAL OF BIOLOGICAL CHEMISTRY
Vol. 278, No. 26, Issue of June 27, pp. 24095–24102, 2003
Printed in U.S.A.

Association of the Cytoskeletal GTP-binding Protein Sept4/H5 with Cytoplasmic Inclusions Found in Parkinson's Disease and Other Synucleinopathies*

Received for publication, February 6, 2003, and in revised form, April 11, 2003
Published, JBC Papers in Press, April 14, 2003, DOI 10.1074/jbc.M301352200

Masafumi Ihara‡§¶, Hidekazu Tomimoto‡, Hitoshi Kitayama§, Yoko Morioka§, Ichiro Akiguchi‡, Hiroshi Shibasaki‡, Makoto Noda§, and Makoto Kinoshita§

From the ‡Department of Neurology, Kyoto University Graduate School of Medicine, Kawahara-cho, Shogoin, Sakyo-ku, Kyoto 606-8507 and the §Department of Molecular Oncology, Kyoto University Graduate School of Medicine, Konoe-cho, Yoshida, Sakyo-ku, Kyoto 606-8501, Japan

α-Synuclein-positive cytoplasmic inclusions are a pathological hallmark of several neurodegenerative disorders including Parkinson's disease, dementia with Lewy bodies, and multiple system atrophy. Here we report that Sept4, a member of the septin protein family, is consistently found in these inclusions, whereas five other septins (Sept2, Sept5, Sept6, Sept7, and Sept8) are not found in these inclusions. Sept4 and α-synuclein can also be co-immunoprecipitated from normal human brain lysates. When co-expressed in cultured cells, FLAG-tagged Sept4 and Myc-tagged α-synuclein formed detergent-insoluble complex, and upon treatment with a proteasome inhibitor, they formed Lewy body-like cytoplasmic inclusions. The tagged Sept4 and α-synuclein synergistically accelerated cell death induced by the proteasome inhibitor, and this effect was further enhanced by expression of another Lewy body-associated protein, synphilin-1, tagged with the V5 epitope. Moreover, co-expression of the three proteins (tagged Sept4, α-synuclein, and synphilin-1) was sufficient to induce cell death. These data raise the possibility that Sept4 is involved in the formation of cytoplasmic inclusions as well as induction of cell death in α-synuclein-associated neurodegenerative disorders.

Parkinson's disease (PD),[1] dementia with Lewy bodies (DLB), and multiple system atrophy (MSA) are neurodegenerative disorders characterized by the formation of similar pathognomonic inclusions in the cytoplasm: namely, Lewy bodies (LBs) in PD and DLB (1–3), and glial cytoplasmic inclusions (GCIs) in MSA (4, 5). These inclusions contain α-synuclein as the major component of the filamentous aggregates. Hence these diseases are classified as synucleinopathies (6).

The importance of α-synuclein in neurodegeneration has been established by the findings that missense mutations in the α-synuclein gene cause familial PD (7, 8) and that transgenic animals overexpressing α-synuclein or its mutants (A30P or A53T) show some phenotypes resembling PD (9–12). LBs also contain ubiquitin (13) and ubiquitin carboxyl-terminal hydrolase-L1 (14), which may be involved in the pathogenesis of PD. Genetic studies on autosomal-recessive juvenile parkinsonism (AR-JP) led to the identification of the responsible gene, *parkin*, which encodes ubiquitin-protein isopeptide ligase (E3) (15). Loss-of-function mutations in *parkin* result in the accumulation of its substrates such as synphilin-1 (16), *O*-glycosylated α-synuclein (17), and Pael receptor (18) and cause neuronal damage without formation of visible inclusions. Synphilin-1 was first identified as an α-synuclein-binding protein (19) and was found to accumulate in LBs (20). Thus, impairment in the ubiquitin-proteasome system and accumulation of α-synuclein and other proteins in the neuronal cytoplasm may represent common molecular mechanisms underlying PD and AR-JP.

Septins are a family of filament-forming guanine nucleotide-binding proteins involved in cytokinesis, exocytosis, and other cellular processes (21–24). At least 10 septin genes, *Sept1–Sept10*, have been identified in mouse as well as human genomes (25). Although septin family members can form co-polymers, their differential expression patterns in mammalian brains indicate some functional diversity among septins (26). Three septins (Sept1, Sept2, and Sept4) are accumulated in tau-based filamentous deposits known as neurofibrillary tangles and glial fibrils in Alzheimer's disease (27). A splice variant of the *Sept4* gene encodes a mitochondrial protein called ARTS (apoptosis-related protein in the transforming growth factor-β signaling pathway), which mediates a pro-apoptotic signal (28). These data support the hypothesis that accumulation of a class of septins may accelerate neurodegeneration. In addition, Sept5 was found to be a substrate of Parkin (29). Sept5 is associated with γ-aminobutyric acidergic synaptic vesicles (26), and excessive expression of Sept5 was found to interfere with regulated exocytosis (22). Thus, accumulation of Sept5 may affect dopamine release in the nigrostriatal system in AR-JP (29, 30).

In this study, we have conducted an immunohistochemical examination of brain tissues from patients afflicted by Parkinson's disease or two other synucleinopathies. We found that Sept4 was co-localized with α-synuclein in LBs/GCIs in all cases. We also analyzed the physical and functional interaction among Sept4, α-synuclein, and synphilin-1 in cultured cells. Our data suggest that these proteins are involved in the formation of cytoplasmic inclusions as well as induction of cell death.

* This work was supported by grants from the Ministry of Education, Culture, Sports, Science and Technology, Japan (to H. T. and M. N.). The costs of publication of this article were defrayed in part by the payment of page charges. This article must therefore be hereby marked "*advertisement*" in accordance with 18 U.S.C. Section 1734 solely to indicate this fact.

¶ To whom correspondence should be addressed. Tel.: 81-75-7513766; Fax: 81-75-7513265; E-mail: ihara@kuhp.kyoto-u.ac.jp.

[1] The abbreviations used are: PD, Parkinson's disease; DLB, dementia with Lewy bodies; MSA, multiple system atrophy; LB, Lewy body; GCI, glial cytoplasmic inclusion; AR-JP, autosomal-recessive juvenile parkinsonism; ARTS, apoptosis-related protein in the transforming growth factor-β signaling pathway; PBS, phosphate-buffered saline; CMV, cytomegalovirus; HA, hemagglutinin; Myc-α-syn, Myc-tagged α-synuclein.

EXPERIMENTAL PROCEDURES

Tissues—Postmortem brain samples were obtained from five patients with PD (age: range, 66–79 years; mean, 74.6 years), two with DLB (69 and 69.0 years), five with MSA (71–78 and 75.0 years), and four with non-neurological diseases (68–81 and 74.5 years) from the Department of Neurology, Kyoto University Hospital. The brain specimens were used for neuropathological investigation after informed consent was obtained from the patients' relatives. The diagnoses of PD, DLB (pure form), and MSA were established on the basis of clinical and neuropathological data according to widely accepted criteria (31–33). After fixation with 4% paraformaldehyde, tissues were dissected. The midbrain and cerebellum were embedded in paraffin and sliced (6 μm in thickness). The frontal lobe, pons, caudatoputamen, and thalamus were freeze-sectioned (20 μm). Mouse brains were obtained from adult male C57Bl/6 mice (25–30 g) after deep anesthesia with sodium pentobarbital (50 mg/kg, intraperitoneal) and transcardial perfusion with phosphate-buffered saline (PBS), using procedures approved by the Animal Use and Care Committee of Kyoto University.

Anti-septin Antibodies, Immunoblot Assay, and Immunohistochemistry—The following polyclonal antibodies were generated as described elsewhere (host animal and antigen are given in parentheses) (21, 26, 27): H5C-2 (rabbit; oligopeptide corresponding to residues 466–478 of mouse Sept4), CRC-3 (guinea pig; residues 358–369 of human Sept5), C10C-3 (guinea pig; residues 400–418 of human Sept7), N5N-1 (rabbit; residues 1–18 of mouse/human Sept2), S6C-3 (guinea pig; residues 413–427 of mouse/human Sept6), and S7C-1 (rabbit; residues 415–429 of human Sept8). The authenticity and specificity of these antibodies were confirmed by antigen adsorption experiments and in some cases by immunoblot assay using cells overexpressing the corresponding gene. Human and mouse brain homogenates (50 μg) were analyzed by standard immunoblot assays (26, 27) using peroxidase-conjugated secondary antibodies and an ECL chemiluminescence kit (Amersham Biosciences). Anti-septin antibodies (see above) or goat anti-α-synuclein antibodies (Santa Cruz Biotechnology) were used as the primary antibodies. Brain sections were stained by immunoperoxidase techniques using Vectastain ABC kits (Vector) with diaminobenzidine tetrahydrochloride as a chromogen or by immunofluorescent staining procedures with fluorescein isothiocyanate- and rhodamine-conjugated secondary antibodies (Molecular Probes).

Plasmids—The coding region of human α-synuclein cDNA was cloned in-frame between the *Eco*RI and *Xho*I sites of the pCMV-Myc vector (Clontech) to express α-synuclein tagged with the Myc epitope at its amino terminus (Myc-α-syn). The coding region of mouse Sept4 cDNA was cloned between the *Eag*I and *Sal*I sites of the pFLAG-CMV-2 vector (Sigma) to express Sept4 tagged with FLAG epitope at its amino terminus (FLAG-Sept4). The coding region of Sept2 was cloned between the *Hin*dIII and *Xba*I sites of the same vector to express FLAG-Sept2. The coding region of human synphilin-1 was cloned into pcDNA3.1/V5-His-TOPO expression vector (Invitrogen) to express synphilin-1 tagged with V5 epitope at its carboxyl terminus (V5-synphilin-1 (34)) (a generous gift from Dr. P. J. McLean). The missense mutations, A30P in α-synuclein and G154V in Sept4, were introduced into the respective wild type cDNAs using the QuikChange site-directed mutagenesis kit (Stratagene). The integrity of each insert cDNA was confirmed by DNA sequencing.

Cell Lines, Transfection, and Fractionation of Cellular Components—Two mouse cell lines, NIH3T3 and N18, were transiently transfected with expression vectors using LipofectAMINE-2000 (Invitrogen). After 24 or 48 h, the cells were rinsed with cold PBS and then lysed using Nonidet P-40 lysis buffer (50 mM Tris-HCl, pH 7.6, 1% Nonidet P-40, 150 mM NaCl, 5 mM EDTA). Fractionation of the subcellular components and subsequent immunoprecipitation were carried out as described previously (18) with minor modifications. In brief, the cell lysates were fractionated by centrifugation at 15,000 × *g* at 4 °C for 30 min, and each fraction was adjusted to the same volume with SDS sample buffer, sonicated (see below), and heat denatured. Equal volumes of these samples were subjected to immunoblot assay, and the amounts of immunoreactive proteins were estimated by densitometry using NIH Image software (version 1.62).

Co-immunoprecipitation—N18 cells (~2 × 10^6) transfected with 2 μg of each plasmid were incubated for 24 h and fractionated as described above. The supernatant fraction was directly immunoprecipitated using anti-FLAG antibodies (Sigma) and protein G-Sepharose beads (Amersham Biosciences). Proteins in the Nonidet P-40-insoluble fraction were solubilized in 1% SDS with the aid of sonication for 20 s and diluted with 10 volumes of Nonidet P-40 lysis buffer. After centrifugation at 15,000 × *g* at 4 °C for 30 min, supernatants from the Nonidet P-40-insoluble fractions were immunoprecipitated. The beads bearing immune complexes were washed three times with 25 volumes of lysis buffer followed by four washings with PBS. The proteins on the beads were solubilized and analyzed by immunoblot assay. For co-immunoprecipitation of endogenous proteins, a human brain sample was homogenized in 4 volumes of PBS containing 320 mM sucrose, 0.1% Triton X-100, and 1 mM phenylmethylsulfonyl fluoride. After centrifugation at 37,000 × *g* at 4 °C for 20 min, the supernatant fraction was subjected to immunoprecipitation with anti-hemagglutinin (HA), anti-α-synuclein (Affiniti Research Products, Exeter, United Kingdom), or anti-Sept4 antibodies. Following five washings with PBS, the precipitates were subjected to immunoblot assay using anti-α-synuclein antibodies.

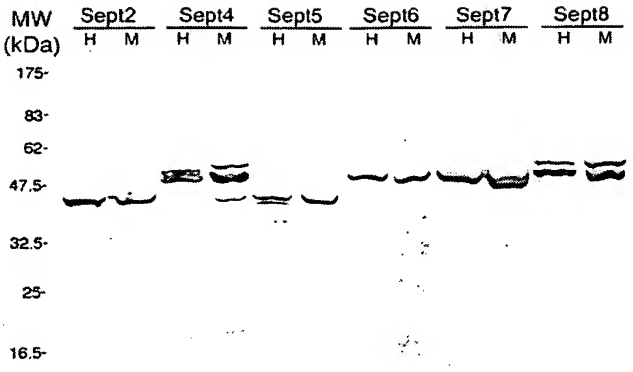

FIG. 1. **Immunoblot detection of six septins in mammalian brains.** Lysates of normal human frontal lobe (*H*) and whole mouse brain (*M*) were analyzed by immunoblot assay with anti-peptide antibodies against the indicated septins. Each lane contained 50 μg of total protein. Note that H5C-2 does not detect the 32-kDa pro-apoptotic Sept4 variant (ARTS).

Immunofluorescent Staining of Cultured Cells and Scoring of Dead Cells—NIH3T3 or N18 cells transfected with three plasmids (each expressing Myc-α-syn, FLAG-Sept4, or V5-synphilin-1) in various combinations were incubated in the absence or presence of 10–20 μM lactacystin for 24 h and immunostained as described previously (21). Mouse monoclonal antibodies against Myc (Sigma), V5 (Invitrogen), or FLAG or rabbit polyclonal antibodies against α-synuclein, FLAG (Sigma), or ubiquitin (Sigma) were used as primary antibodies. Fluorescein isothiocyanate- or rhodamine-conjugated anti-mouse IgG or anti-rabbit IgG was used as secondary antibodies. Dead cells were scored after brief staining with 0.2% trypan blue (Invitrogen) or with 1.0 μg/ml annexin V-enhanced green fluorescent protein (Clontech) plus 2.5 μg/ml propidium iodide (Clontech).

Ubiquitination Assay—NIH3T3 cells (~5 × 10^4) transfected with 1 μg of FLAG-Sept4 expression vector were incubated in growth medium for 24 h and then in medium with or without 20 μM lactacystin for an additional 16 h. Fractionated cell lysates were analyzed directly, or after immunoprecipitation with anti-FLAG antibodies, by immunoblot assay using antibodies against ubiquitin or FLAG.

Statistics—Quantitative data were collected in at least three independent experiments. Significance of difference between data groups was assessed by Student's *t* test using StatView II software (version 5.0 for Macintosh, SAS Institute). *p* values smaller than 0.05 were considered significant.

RESULTS

Expression of Six Septins in Human and Mouse Brains—We first examined the expression of six septins in the normal human frontal lobe and mouse whole brain by immunoblot assay using specific antibodies (Fig. 1). All six septins were detected in the human and mouse brains. The anti-Sept4 antibody (H5C-2) detected three major bands of 53, 51, and 49 kDa in the human brain; this antibody does not recognize the 32-kDa pro-apoptotic Sept4 variant, ARTS (28), because ARTS lacks the carboxyl-terminal region of Sept4 where the epitope for H5C-2 resides.

Sept4 Is Commonly Associated with α-Synuclein-based Cytoplasmic Inclusions—Having established the expression of six

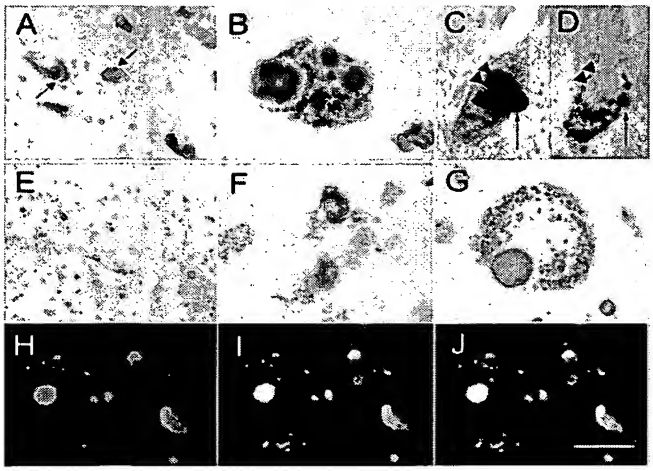

FIG. 2. **Immunostaining for Sept4 and α-synuclein of brain sections from patients with Parkinson's disease (*A–D*) and dementia with Lewy bodies (*E–J*).** *A* and *B*, pigmented nerve cells with Sept4-positive (*red*) LBs (*arrows*). *C* and *D*, adjacent sections showing a pigmented nerve cell with LBs (*arrows*) immunostained for α-synuclein (*C*) and Sept4 (*D*). Note that the α-synuclein-positive pale body is weakly Sept-4-positive (*arrowheads*). *E* and *F*, numerous non-pyramidal neurons with Sept4-positive (*red*) LBs in the cingulate cortex. *G*, a pigmented nerve cell with a Sept4-positive LB in the substantia nigra. *H–J*, cortical LBs double stained for Sept4 (*H*, *red*) and α-synuclein (*I*, *green*) and the merged image (*J*). *Scale bar* = 100 μm (*A* and *E*), 40 μm (*C*, *D*, and *H–J*), and 20 μm (*B*, *F*, and *G*).

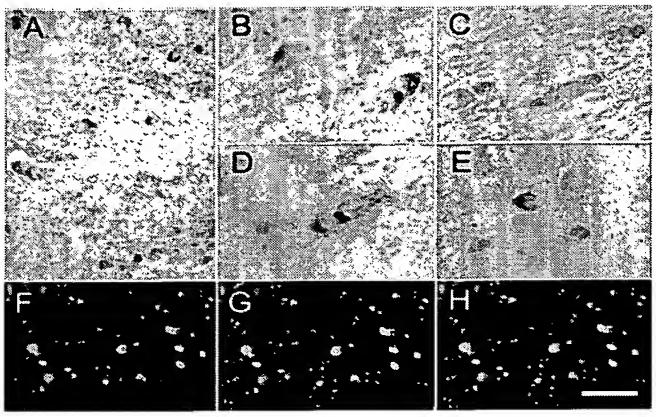

FIG. 3. **Sept4 is a component of α-synuclein-based cytoplasmic inclusions in multiple system atrophy.** *A–E*, Sept4-positive GCIs in the thalamus (*A* and *B*), cerebellum (*C*), pontine base (*D*), and putamen (*E*). *F–H*, GCIs double stained for Sept4 (*F*, *red*) and α-synuclein (*G*, *green*) and the merged image (*H*). *Scale bar*: 40 μm (*A* and *F–H*) and 20 μm (*B–E*).

septins in the normal mouse brain and human frontal lobe, we next studied the expression of these septins in the postmortem brain samples from patients with neurodegenerative disorders. Notably, in all of the PD cases we tested (n = 5), nigral LBs were found to be stained positive with the anti-Sept4 antibody (H5C-2) (Fig. 2, *A* and *B*). Preadsorption of H5C-2 with its cognate antigen abolished this staining (data not shown). Double staining of serial sections indicated that 70–80% of α-synuclein-positive LBs were Sept4-positive (data not shown). Distribution of these two proteins, however, looked different; Sept4-staining was low in the corona of LB where α-synuclein staining was most intense (Fig. 2, *C* and *D*). Sept4 was also found in another type of α-synuclein-positive structures termed pale bodies (Fig. 2, *C* and *D*, *arrowheads*) (3). Such aberrant structures containing Sept4 were not found in nigral neurons in normal control brains (n = 4; data not shown). All six septins examined are expressed in normal substantia nigra (26), and yet none of them except Sept4 was found to be accumulated in LBs, suggesting selective incorporation of Sept4 into LBs (data not shown).

Sept4 was also detected in the cortical and nigral LBs in brains with DLB (n = 2, Fig. 2, *E–G*). The Sept4-positive cortical LBs frequently found in the small-to-medium-size, non-pyramidal neurons in deeper cortical layers lacked distinct core (Fig. 2, *E* and *F*), whereas the nigral LBs (Fig. 2*G*) were similar in morphology to those in PD (see above). Immunofluorescent double staining revealed that most of the α-synuclein-positive inclusions found in DLB brains were Sept4-positive. In cortical LBs, distribution of Sept4 and α-synuclein appeared to be tightly overlapped (Fig. 2, *H–J*). Again, none of the septins examined except Sept4 was found to accumulate in the nigral and cortical LBs in DLB brains.

Our previous studies indicate that Sept4 is expressed in both neurons and glial cells (26). Consistent with this observation, we found Sept4-positive GCIs in several regions including the cerebellum, pons, caudatoputamen, and thalamus in brains with MSA (n = 5, Fig. 3). These findings demonstrate common and selective association of Sept4 with the inclusions in synucleinopathies.

Physical Interaction between Sept4 and α-Synuclein in the Brain and in Cultured Cells—To test the possible interaction between Sept4 and α-synuclein *in vivo*, human brain homogenate was immunoprecipitated with anti-HA (negative control), anti-α-synuclein, or anti-Sept4 antibodies and then subjected to immunoblot analysis with anti-α-synuclein antibodies (Fig. 4*A*). A fraction of α-synuclein was consistently pulled down with Sept4, indicating direct or indirect physical interaction between Sept4 and α-synuclein *in vivo*.

To analyze the molecular nature of this interaction, mouse cell lines (N18 neuroblastoma and NIH3T3 fibroblast) were co-transfected with a plasmid vector expressing α-synuclein tagged with Myc epitope (Myc-α-syn) and a second vector expressing either the normal Sept4, a mutant Sept4 ($Sept4^{G154V}$), or the normal Sept2, each tagged with the FLAG epitope (Fig. 4, *B* and *C*). We chose to use short epitope tags (Myc and FLAG) to reduce the probability of generating insoluble fusion proteins, as has been reported for the green fluorescent protein tag (34). $Sept4^{G154V}$ has a missense mutation in its "P-loop" domain and shows reduced guanine nucleotide-binding activity (21, 28, 35). The transfected cells were lysed in a buffer containing 1% Nonidet P-40, and the subcellular components were separated into Nonidet P-40-soluble and -insoluble fractions. We subjected each fraction directly or after immunoprecipitation with anti-FLAG antibodies to the immunoblot assay using anti-Myc antibodies (to detect Myc-α-syn) or anti-FLAG antibodies (to detect FLAG-septins). From the Nonidet P-40-soluble fraction, Myc-α-syn co-precipitated with FLAG-Sept4 (Fig. 4*B*, *middle panel*, *lane 4*), indicating physical interaction between tagged α-synuclein and Sept4 in cultured cells. Myc-α-syn co-precipitated with FLAG-$Sept4^{G154V}$ or FLAG-Sept2 was less than that co-precipitated with FLAG-Sept4 (Fig. 4*B*, *middle panel*; compare *lanes 4*, *6*, and *8*) even though the total amount of Myc-α-syn in the sample of FLAG-$Sept4^{G154V}$- or FLAG-Sept2-transfected cells was comparable with, if not greater than, that in the sample of FLAG-Sept4-transfected cells (Fig. 4*B*, *top panel*; compare *lanes 6* and *8* with *lane 4*). This may reflect the difference in the levels of FLAG-tagged septins present in these samples and/or the difference in their ability to be incorporated into the molecular complexes. Nevertheless, the wild type FLAG-Sept4 construct was the most efficient among the three septin constructs we tested in bring-

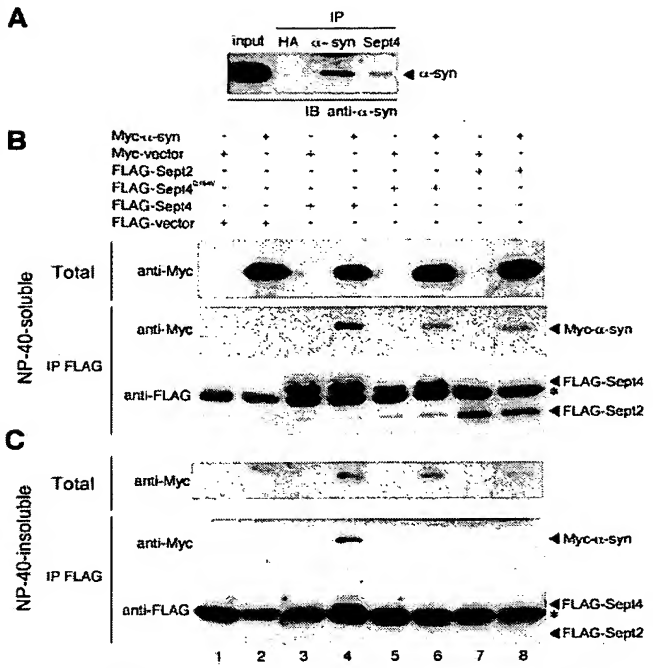

FIG. 4. **Sept4 and α-synuclein form insoluble complexes.** *A*, human brain homogenates were subjected to immunoprecipitation (*IP*) with anti-HA (negative control), anti-α-synuclein, or anti-Sept4 antibodies followed by immunoblot (*IB*) detection with anti-α-synuclein antibodies. *B* and *C*, co-immunoprecipitation of FLAG-Sept4 and Myc-α-synuclein (*Myc-α-syn*). N18 mouse neuroblastoma cells were co-transfected with the indicated expression vectors. After a 36-h incubation, the cells were lysed with buffer containing 1% Nonidet P-40 and fractionated into soluble (*B*) and insoluble fractions (*C*). Each fraction was subjected to immunoprecipitation with anti-FLAG antibodies (*IP FLAG*) followed by immunoblot detection using anti-Myc to detect Myc-α-syn (*middle panels*) or anti-FLAG to detect FLAG-Sept4 or FLAG-Sept2 (*bottom panels*). The *asterisk* indicates the position of the immunoglobulin heavy chain. All three experiments were repeated three times with similar results.

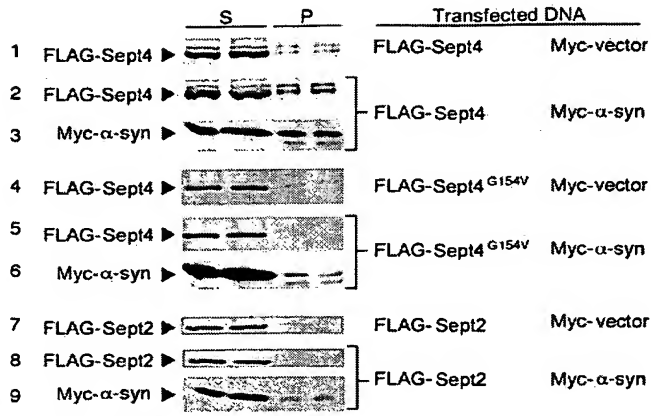

FIG. 5. **FLAG-Sept4 and Myc-α-syn form detergent-insoluble complexes.** NIH3T3 mouse fibroblast cells were transfected with the indicated expression vectors. After a 48-h incubation, the cells were lysed and fractionated with buffer containing 1% Nonidet P-40. The Nonidet P-40-soluble (*S*) (duplicate samples in *left two lanes*) and -insoluble (*P*) (duplicate samples in *right two lanes*) fractions were subjected to immunoblot analysis using anti-FLAG (to detect FLAG-Sept4 or FLAG-Sept2) or anti-Myc antibodies (to detect Myc-α-syn). Note that proteins in the Nonidet P-40-insoluble fractions were solubilized directly with SDS sample buffer in this experiment, which is different from the procedure employed in the experiments shown in Fig. 4 (see "Experimental Procedures" for more detail).

ing down Myc-α-syn from the Nonidet P-40-soluble fraction.

The amount of Myc-α-syn found in the Nonidet P-40-insoluble fraction was small when expressed alone (Fig. 4*C*, *top panel*, *lane 2*) but was increased when FLAG-Sept4 or FLAG-Sept4^{G154V} was co-expressed (Fig. 4*C*, *top panel*, *lanes 4* and *6*); this effect was minimal when FLAG-Sept2 was co-expressed (Fig. 4*C*, *top panel*, *lane 8*). Interestingly, immunoprecipitable FLAG-tagged protein and the associated Myc-α-syn came to the Nonidet P-40-insoluble fraction only when FLAG-Sept4 and Myc-α-syn were co-expressed (Fig. 4*C*, *bottom two panels*, *lane 4*), suggesting that FLAG-Sept4 and Myc-α-syn become insoluble to Nonidet P-40 in a co-operative manner. In contrast, FLAG-Sept4^{G154V} and FLAG-Sept2 failed to bring Myc-α-syn to the Nonidet P-40-insoluble fraction (Fig. 4*C*, *bottom two panels*, *lanes 6* and *8*). We obtained similar results with NIH3T3 cells (data not shown).

FLAG-Sept4 and Myc-α-syn Become Detergent-insoluble when Co-expressed—The above observations suggest that FLAG-Sept4 and Myc-α-syn are soluble when expressed alone but both become insoluble when they are co-expressed. To confirm this model, NIH3T3 cells transfected with plasmids in various combinations were lysed in buffer containing 1% Nonidet P-40, and partition of each protein into the supernatant (*S*) and pellet (*P*) fractions was estimated by immunoblot assay (Fig. 5). Consistent with the above observation (Fig. 4*C*), co-expression of Myc-α-syn brought more FLAG-Sept4 into the pellet fraction (Fig. 5, compare *panels 1* and *2*). In contrast, Myc-α-syn showed little effects on the solubility of FLAG-Sept4^{G154V} or FLAG-Sept2 under these conditions (Fig. 5, compare *panels 4* and *5*, and *panels 7* and *8*). Reciprocally, co-expression of FLAG-Sept4, but not FLAG-Sept4^{G154V} or FLAG-Sept2, brought more Myc-α-syn into the insoluble fraction (Fig. 5, compare *panels 3*, *6*, and *9*). These data demonstrate the bidirectional nature of the interaction between FLAG-Sept4 and Myc-α-syn in bringing these proteins into the Nonidet P-40-insoluble fraction.

Localization and Biological Activity of Overexpressed FLAG-Sept4 and Myc-α-syn in Cultured Cells—To determine the subcellular localization of FLAG-Sept4 and Myc-α-syn, we performed immunofluorescent staining of transfected cells using anti-FLAG and anti-Myc antibodies (Fig. 6*A*). FLAG-Sept4 and Myc-α-syn were diffusely distributed in the cytoplasm with apparent accumulation and co-localization at the cortex or periphery of the cells (Fig. 6*A*, *top row*). After treatment with a proteasome inhibitor, lactacystin, a subset (~30%) of the cells contained punctate aggregates at the cell periphery and/or rods in the cytoplasmic protrusions (Fig. 6*A*, *middle row*). Interestingly, a fraction (~5%) of doubly transfected, lactacystin-treated cells contained large, double-positive structures reminiscent of LBs (Fig. 6*A*, *bottom row*). Such a structure was not found in cells expressing FLAG-Sept4 alone or Myc-α-syn alone. Aggregates were rare in the cells expressing Myc-α-syn alone (Fig. 6*B*), FLAG-Sept4 alone (<0.5%, data not shown), or Myc-α-syn plus FLAG-Sept4^{G154V} or FLAG-Sept2 (<5%, data not shown).

Interestingly, a dye exclusion assay using trypan blue showed that the cells expressing both FLAG-Sept4 and Myc-α-syn were more sensitive to cytotoxicity by lactacystin as compared with the cells expressing one of the proteins alone or transfected with empty vectors (Fig. 6*C*). Separate experiments employing annexin V-enhanced green fluorescent protein and propidium iodide to stain dying cells also showed similar results (data not shown). Hence, FLAG-Sept4 and Myc-α-syn were co-operative in making cells vulnerable to the stress induced by proteasome inhibition.

The FLAG(Sept4)/Myc(α-syn) double-positive aggregates

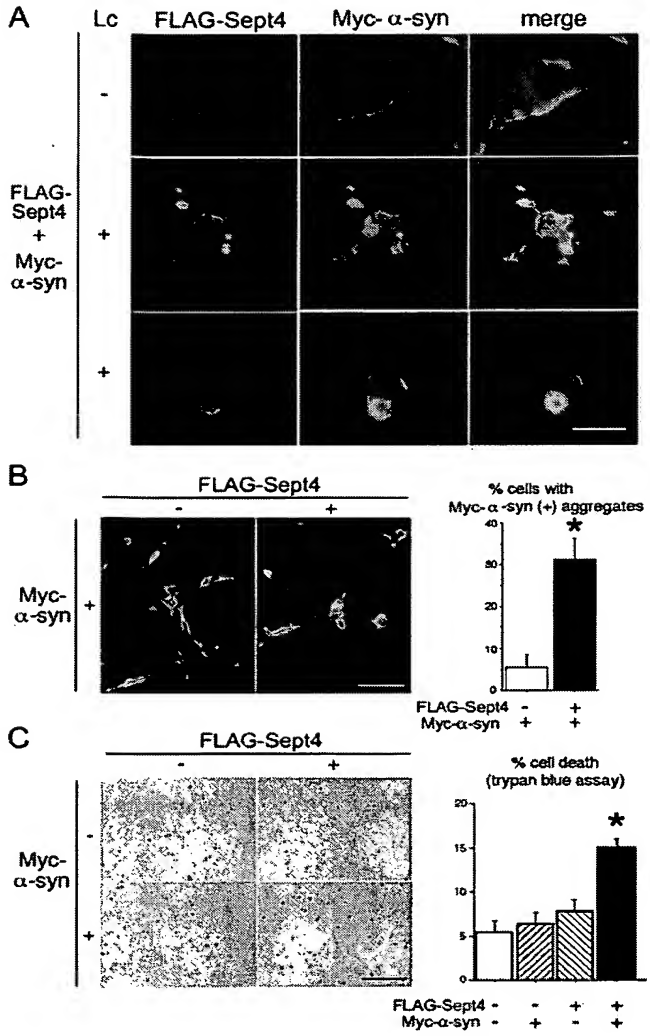

FIG. 6. **FLAG-Sept4 and Myc-α-syn synergistically induce aggregate formation and make cells vulnerable to the cytotoxic effects of lactacystin.** *A*, NIH3T3 cells co-transfected with plasmids expressing FLAG-Sept4 and Myc-α-syn were incubated in the absence (−) or presence (+) of lactacystin (*Lc*) followed by immunostaining with anti-FLAG (*red*) or anti-Myc (*green*) antibodies. Merged images are also shown. *Scale bar* = 5 μm (*upper six panels*) and 7.5 μm (*lower three panels*). *B*, NIH3T3 cells co-transfected with a vector expressing Myc-α-syn plus either FLAG-vector (−) or a vector expressing FLAG-Sept4 (+) were treated with lactacystin. After a 24-h incubation and immunofluorescent staining with anti-Myc antibodies, the proportion of cells harboring fluorescent aggregates among the total of 800 Myc-α-syn-positive cells was scored. *Error bars* represent S.D. from three independent experiments. *Scale bar* = 20 μm. *, $p = 0.0016$ comparing cells expressing both Myc-α-syn and FLAG-Sept4 to those expressing Myc-α-syn alone. *C*, NIH3T3 cells co-transfected with the indicated expression vectors ("−" indicates empty vector) were treated with lactacystin for 24 h and then stained with trypan blue. The proportion of blue cells among the total of 1000 cells was scored under a phase-contrast microscope. *Error bars* represent S.D. from three independent experiments. *, $p < 0.002$ comparing cells co-transfected with Myc-α-synuclein and FLAG-Sept4 to those transfected with other indicated combinations. *Scale bar* = 100 μm. All experiments were repeated three times with similar results.

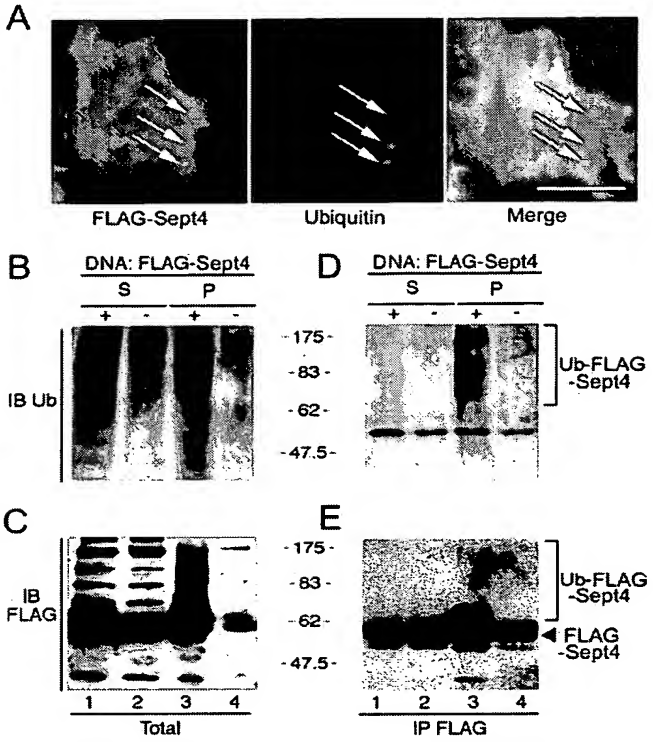

FIG. 7. **Proteasome inhibition results in accumulation of insoluble, ubiquitinated FLAG-Sept4.** *A*, N18 cells (~5 × 10^4) expressing FLAG-Sept4 and Myc-α-synuclein were incubated in the presence of a proteasome inhibitor (10 μM lactacystin) for 24 h followed by immunostaining with anti-FLAG (*A*, *green*) or anti-ubiquitin (*B*, *red*) antibodies. Merged images are also shown. *Scale bar* = 5 μm. *B–E*, NIH3T3 cells (~5 × 10^4) expressing FLAG-Sept4 were treated with 20 μM lactacystin for 16 h, lysed in 1% Nonidet P-40 lysis buffer, and analyzed by immunoblot assay using anti-ubiquitin (*IB Ub*) antibodies. Accumulation of ubiquitinated proteins was detected in both the Nonidet P-40-soluble (*S*) and -insoluble (*P*) fractions after lactacystin treatment (*B*, *lanes 1* and *3*). On the immunoblots treated with anti-FLAG antibodies (to detect Sept4), broad smears in the high molecular mass range, which probably represent FLAG-Sept4 molecules ubiquitinated to various degrees, were found only in the Nonidet P-40-insoluble fraction (*C*, *lane 3*). The discrete bands in the high molecular mass range of the Nonidet P-40-soluble fraction (*C*, *lanes 1* and *2*) are probably nonspecific, because they were also seen in vector-transfectants (data not shown). Immunoprecipitation of FLAG-Sept4 with anti-FLAG antibodies followed by immunoblot detection with anti-ubiquitin (*D*) or anti-FLAG (*E*) more clearly demonstrated that lactacystin treatment increases the amount of ubiquitinated FLAG-Sept4 only in the Nonidet P-40-insoluble fractions (*D* and *E*, *lane 3*).

also contained ubiquitin (Fig. 7*A*), and ubiquitinated FLAG-Sept4 was found predominantly in detergent-insoluble fractions (Fig. 7, *B–E*). Thus, FLAG-Sept4 can be ubiquitinated; this may occur in insoluble molecular complexes, or once ubiquitinated, FLAG-Sept4 may rapidly be incorporated into such complexes.

We also generated and tested the activities of a Myc-α-syn expression plasmid harboring a missense mutation (A30P) that has been found in familial PD cases (8). Interestingly, the amounts of FLAG-Sept4 and Myc-α-syn in the anti-FLAG-immunoprecipitates from Nonidet P-40-soluble fractions were slightly but consistently greater when Myc-α-syn^{A30P} was used (Fig. 8*A*). Furthermore, cells co-expressing FLAG-Sept4 and Myc-α-syn^{A30P} were more sensitive to lactacystin toxicity than cells expressing FLAG-Sept4 plus wild type Myc-α-syn (Fig. 8*C*).

Effects of V5-Synphilin-1—It has been reported that synphilin-1 induces cytoplasmic inclusions when co-expressed with α-synuclein in HEK293 cells (19). When Myc-α-syn and synphilin-1 tagged with another oligopeptide epitope (V5) were co-expressed in NIH3T3 cells, α-syn/V5 double-positive cyto-

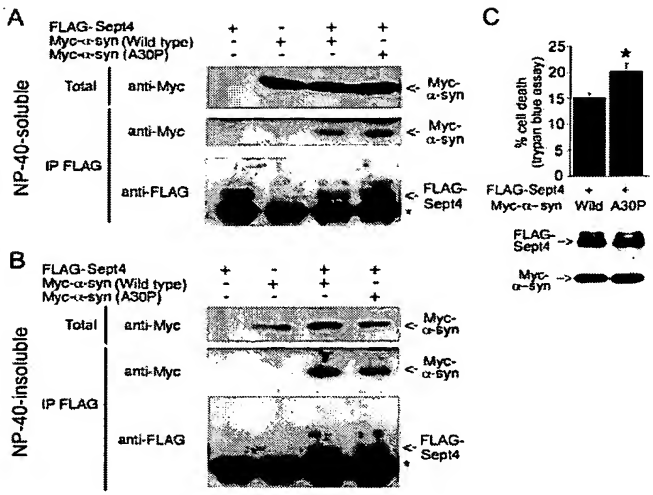

FIG. 8. **Co-immunoprecipitation of Sept4 and wild type or A30P α-synuclein.** *A* and *B*, NIH3T3 cells were co-transfected with the indicated expression vectors. After a 36-h incubation, the cells were lysed with buffer containing 1% Nonidet P-40 and fractionated into soluble (*A*) and insoluble (*B*) fractions. Each fraction was subjected to immunoprecipitation with anti-FLAG antibodies (*IP FLAG*) followed by immunoblot detection using anti-Myc to detect Myc-α-synuclein (*middle panels*) or anti-FLAG to detect FLAG-Sept4 (*lower panels*). The *asterisk* indicates the position of the immunoglobulin heavy chain. These experiments were repeated twice with similar results. *C*, NIH3T3 cells co-transfected with the indicated expression vectors were treated with lactacystin for 24 h and then stained with trypan blue. The proportion of blue cells among a total of 1000 cells was scored under a microscope. *Error bars* represent S.D. from three independent experiments. *, $p = 0.045$ comparing cells expressing wild type and A30P α-synuclein. The expression levels of the total FLAG-Sept4 and Myc-α-syn proteins, as detected by immunoblot assay using anti-FLAG and anti-Myc antibodies, respectively (*bottom two panels*), were not greatly different between the two transfectant populations.

plasmic inclusions formed (Fig. 9*A*), supporting the previous finding. Interestingly, when FLAG-Sept4 was additionally expressed in this system, larger inclusions with LB-like morphology formed (Fig. 9*B*, *upper panels*). These round inclusions were frequently accompanied by satellite inclusions with irregular shapes (Fig. 9*B*, *lower panels*), which are reminiscent of pale bodies, putative precursors of LB found in PD neurons (see Fig. 2, *C* and *D*) (3). These irregular inclusions were FLAG (Sept4)-positive but V5 (synphilin-1)-negative (Fig. 9*B*, *lower panels*). FLAG-Sept4 and V5-synphilin-1 could not be co-immunoprecipitated, and they did not form inclusions in the absence of Myc-α-syn (data not shown).

Expression of V5-synphilin-1 itself was cytotoxic, especially when combined with lactacystin treatment (Fig. 9*C*, compare *bars 2* and *4*; $p = 0.0037$). Although additional expression of Myc-α-syn had little effect on cytotoxicity (Fig. 9*C*, compare *bars 3* and *4* with *bars 5* and *6*), additional expression of Myc-α-syn plus FLAG-Sept4 resulted in significant enhancement of cytotoxicity, especially when combined with lactacystin treatment (Fig. 9*C*; compare *bars 4* and *8*, $p = 0.046$). The effect of V5-synphilin-1 in enhancing the cytotoxicity exerted by FLAG-Sept4 and Myc-α-syn was significant both in the absence and presence of lactacystin (Fig. 9*C*; compare *bars 7* and *9*, $p = 0.029$, and *bars 8* and *10*, $p = 0.015$). Taken together, these findings raise the possibility that Sept4 has the potential to cooperate with α-synuclein and synphilin-1 to induce cytoplasmic inclusions and cell death.

DISCUSSION

An important finding in this study is that Sept4 is accumulated in cytoplasmic inclusions found in three major synucleinopathies, PD, DLB, and MSA. In nigral LBs, Sept4 is found predominantly in the central cores and α-synuclein in the peripheral portions. Possible explanations for this finding include: (i) indirect association between Sept4 and α-synuclein; (ii) selective association of one of the proteins with a subset of the other due, for instance, to differential modification or conformational change; and (iii) epitope masking in specific area of LBs. In cultured cells, FLAG-Sept4 and Myc-α-syn were cooperatively incorporated into the Nonidet P-40-insoluble fraction, and upon proteasome inhibition or expression of V5-synphilin-1, they participated in the formation of LB-like cytoplasmic inclusions and promotion of cell death. Taken together, our findings *in vivo* and *in vitro* support the idea that endogenous Sept4 and α-synuclein are actively involved in LB formation and promotion of cell death. Furthermore, our finding that pale body-like cytoplasmic aggregates did not contain V5-synphilin-1 (Fig. 9) suggests that interaction between Sept4 and α-synuclein may be an early event during LB formation. In fact, a recent report indicates that synphilin-1 is negative in pale bodies (36).

Results with overexpression of tagged proteins in cultured cells cannot be directly extrapolated to the pathological conditions in the brain. Such experiments *in vitro*, however, have their own advantages, and if supported by pathological evidence, they may shed light on the role of particular molecules in human disorders. The most obvious and important limitation of pathological evidence is that it completely depends on the availability of samples and that it is always retrospective. Furthermore, immunohistological evidence heavily depends on the quality of the antibodies used; thus the possibility of cross-reaction or epitope masking is often hard to exclude. Antibodies against epitope tags (*e.g.* FLAG, Myc, and V5) are high in affinity and specificity, so that clear-cut experimental evidence can be obtained. Although the effects of the extra peptide on the conformation of tagged protein cannot be completely excluded, we found no evidence that the tagged proteins tended to be insoluble when expressed alone. Our immunohistochemical evidence (Figs. 2 and 3) as well as the data obtained with specific antibodies (Fig. 4*A*) make it further unlikely that the observed interactions between the tagged proteins represent mere artifacts.

The primary structure of Sept4 is unique among septins in that it has an extended amino-terminal region (37). The largest form of Sept4 (478 amino acid residues) is more than 100 residues longer than Sept5 (369 residues). This extended region, which shares no homology with any other protein in the current data base, may confer unique biochemical properties on Sept4. In contrast, the remaining portion of Sept4 is highly homologous (78% identical) to Sept5, a known target for Parkin (29, 30). Our data indicate that upon proteasome inhibition, Myc-α-syn and ubiquitinated FLAG-Sept4 accumulate in the detergent-insoluble fraction (Fig. 7), which probably corresponds, at least in part, to the visible cytoplasmic inclusions (Fig. 6). Whether the FLAG-Sept4 ubiquitination in this system is mediated by endogenous Parkin or by some other ubiquitin protein ligase remains to be clarified.

Sept4 and synphillin-1 share three properties in common: they can be co-immunoprecipitated with α-synuclein (19), ubiquitinated by Parkin (16) or unknown ubiquitin ligase, and concentrated in the LB cores (20). In the cell culture model, we demonstrated that FLAG-Sept4 and V5-synphilin-1 can co-localize in the Myc-α-syn-based cytoplasmic inclusions and that the three proteins can synergistically exert cytotoxicity. The relationship between inclusion body formation and cell death in synucleinopathies is currently unknown, but we can envisage two possibilities: 1) Sept4, α-synuclein, and synphilin-1 syner-

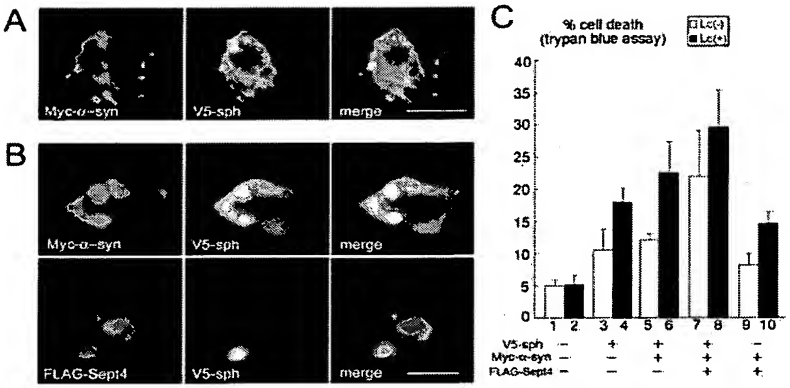

FIG. 9. **FLAG-Sept4 cooperates with Myc-α-syn and V5-synphilin-1 in inducing inclusions and cell death.** *A*, NIH3T3 cells co-transfected with plasmids expressing Myc-α-syn and V5-synphilin-1 (*V5-sph*) were immunostained with anti-α-synuclein (*red*) or anti-V5 antibodies (*green*). The merged image is also shown. *Scale bar* = 5 μm. *B*, NIH3T3 cells transfected with plasmids expressing V5-synphilin-1, Myc-α-syn, and FLAG-Sept4 were immunostained with anti-α-synuclein (*red*), anti-V5 (*green*), or anti-FLAG antibodies (*red*). Merged images are also shown. *Scale bar* = 5 μm. *C*, NIH3T3 cells transfected with the indicated expression vectors ("−" indicates empty vector) were treated with lactacystin (*Lc*) for 24 h and then stained with trypan blue. The proportion of blue cells among the total of 1000 cells was scored under a microscope. *Error bars* represent S.D. from three independent experiments. Differences were significant ($p < 0.05$) between the following data sets: *bars 1 versus 5, 1 versus 7, 7 versus 9, 2 versus 4, 2 versus 6, 2 versus 8, 4 versus 8,* and *8 versus 10*. All experiments were repeated three times with similar results.

gistically form insoluble aggregates or inclusions that trigger cell death; or 2) Sept4, α-synuclein, and synphilin-1 form soluble toxic complexes that trigger cell death unless enclosed into inclusions. The fact that AR-JP shows earlier onset than the other types of PD and that neurons affected in AR-JP do not contain LBs (38) is consistent with the second model. Recent reports that soluble α-synuclein complexes are linked to neurotoxicity in dopaminergic neurons (39) and that inclusion body formation and cell death are mutually exclusive phenomena in PC12 cells (40) also support this model. Our data on the Myc-α-syn^{A30P} mutant (Fig. 8) indicate an apparent correlation between the increase in Nonidet P-40-soluble FLAG-Sept4·Myc-α-syn complexes and cytotoxicity, raising the possibility that the Nonidet P-40-insoluble material itself is not the toxic entity. This finding may provide an additional support to the second model. However, α-synuclein aggregates/inclusions seem to mechanically damage neurons in an α-synuclein transgenic mice model (10–12, 41). More indirect mechanisms are also possible; accumulated Sept4, α-synuclein, and synphilin-1 could sequester their ubiquitin-protein ligases (*e.g.* Parkin) into the inclusions (42). Alternatively, sequestration of Sept4 from the cytoplasm to inclusions could affect neuronal function by destabilizing actin cytoskeleton (24). In fact, impaired actin turnover is implicated in neurodegenerative diseases such as primary dystonia (43) and Alzheimer's disease (44). These hypotheses based on our findings should be tested *in vivo* in future studies.

We reported previously that Sept4 and two other septins are present in the tau-based neurofibrillary tangles in Alzheimer's disease (27). Because PD and Alzheimer's disease show considerable overlap in their clinicopathological features, it has been proposed that common molecular mechanisms may underlie synucleinopathies and tauopathies (41, 45). In this regard, Sept4 is unique in its association with the aberrant protein depositions in both types of diseases. Further studies on the biochemical properties and physiological functions of Sept4 may therefore provide important insights into the common mechanism underlying diverse neurodegenerative disorders.

Acknowledgments—We thank S. Tanaka for NACP/α-synuclein cDNA, K. Kato for H5/Sept4 cDNA, P. J. McLean for synphilin-1 cDNA, E. Nishimoto and H. Nakabayashi for technical assistance, and M. Fukuda and A. Miyazaki for secretarial assistance. We also thank B. T. Hyman and D. B. Alexander for the critical review of our manuscript.

REFERENCES

1. Spillantini, M. G., Schmidt, M. L., Lee, V. M., Trojanowski, J. Q., Jakes, R., and Goedert, M. (1997) *Nature* **388**, 839–840
2. Baba, M., Nakajo, S., Tu, P. H., Tomita, T., Nakaya, K., Lee, V. M., Trojanowski, J. Q., and Iwatsubo, T. (1998) *Am. J. Pathol.* **152**, 879–884
3. Irizarry, M. C., Growdon, W., Gomez-Isla, T., Newell, K., George, J. M., Clayton, D. F., and Hyman, B. T. (1998) *J. Neuropathol. Exp. Neurol.* **57**, 334–337
4. Tu, P. H., Galvin, J. E., Baba, M., Giasson, B., Tomita, T., Leight, S., Nakajo, S., Iwatsubo, T., Trojanowski, J. Q., and Lee, V. M. (1998) *Ann. Neurol.* **44**, 415–422
5. Spillantini, M. G., Crowther, R. A., Jakes, R., Cairns, N. J., Lantos, P. L., and Goedert, M. (1998) *Neurosci. Lett.* **251**, 205–208
6. Galvin, J. E., Lee, V. M., and Trojanowski, J. Q. (2001) *Arch. Neurol.* **58**, 186–190
7. Polymeropoulos, M. H., Lavedan, C., Leroy, E., Ide, S. E., Dehejia, A., Dutra, A., Pike, B., Root, H., Rubenstein, J., Boyer, R., Stenroos, E. S., Chandrasekharappa, S., Athanassiadou, A., Papapetropoulos, T., Johnson, W. G., Lazzarini, A. M., Duvoisin, R. C., Di Iorio, G., Golbe, L. I., and Nussbaum, R. L. (1997) *Science* **276**, 2045–2047
8. Kruger, R., Kuhn, W., Muller, T., Woitalla, D., Graeber, M., Kosel, S., Przuntek, H., Epplen, J. T., Schols, L., and Riess, O. (1998) *Nat. Genet.* **18**, 106–108
9. Masliah, E., Rockenstein, E., Veinbergs, I., Mallory, M., Hashimoto, M., Takeda, A., Sagara, Y., Sisk, A., and Mucke, L. (2000) *Science* **287**, 1265–1269
10. Giasson, B. I., Duda, J. E., Quinn, S. M., Zhang, B., Trojanowski, J. Q., and Lee, V. M. (2002) *Neuron* **34**, 521–533
11. Lee, M. K., Stirling, W., Xu, Y., Xu, X., Qui, D., Mandir, A. S., Dawson, T. M., Copeland, N. G., Jenkins, N. A., and Price, D. L. (2002) *Proc. Natl. Acad. Sci. U. S. A.* **99**, 8968–8973
12. Neumann, M., Kahle, P. J., Giasson, B. I., Ozmen, L., Borroni, E., Spooren, W., Muller, V., Odoy, S., Fujiwara, H., Hasegawa, M., Iwatsubo, T., Trojanowski, J. Q., Kretzschmar, H. A., and Haass, C. (2002) *J. Clin. Investig.* **110**, 1429–1439
13. Kuzuhara, S., Mori, H., Izumiyama, N., Yoshimura, M., and Ihara, Y. (1998) *Acta Neuropathol.* **75**, 345–353
14. Lowe, J., McDermott, H., Landon, M., Mayer, R. J., and Wilkinson, K. D. (1990) *J. Pathol.* **161**, 153–160
15. Shimura, H., Hattori, N., Kubo, S., Mizuno, Y., Asakawa, S., Minoshima, S., Shimizu, N., Iwai, K., Chiba, T., Tanaka, K., and Suzuki, T. (2000) *Nat. Genet.* **25**, 302–305
16. Chung, K. K., Zhang, Y., Lim, K. L., Tanaka, Y., Huang, H., Gao, J., Ross, C. A., Dawson, V. L., and Dawson, T. M. (2001) *Nat. Med.* **7**, 1144–1150
17. Shimura, H., Schlossmacher, M. G., Hattori, N., Frosch, M. P., Trockenbacher, A., Schneider, R., Mizuno, Y., Kosik, K. S., and Selkoe, D. J. (2001) *Science* **293**, 263–269
18. Imai, Y., Soda, M., Inoue, H., Hattori, N., Mizuno, Y., and Takahashi, R. (2001) *Cell* **105**, 891–902
19. Engelender, S., Kaminsky, Z., Guo, X., Sharp, A. H., Amaravi, R. K., Kleiderlein, J. J., Margolis, R. L., Troncoso, J. C., Lanahan, A. A., Worley, P. F., Dawson, V. L., Dawson, T. M., and Ross, C. A. (1999) *Nat. Genet.* **22**, 110–114
20. Wakabayashi, K., Engelender, S., Yoshimoto, M., Tsuji, S., Ross, C. A., and Takahashi, H. (2000) *Ann. Neurol.* **47**, 521–523

21. Kinoshita, M., Kumar, S., Mizoguchi, A., Ide, C., Kinoshita, A., Haraguchi, T., Hiraoka, Y., and Noda, M. (1997) *Genes Dev.* **11,** 1535–1547
22. Beites, C. L., Xie, H., Bowser, R., and Trimble, W. S. (1999) *Nat. Neurosci.* **2,** 434–439
23. Field, C. M., and Kellogg, D. (1999) *Trends Cell Biol.* **9,** 387–394
24. Kinoshita, M., Field, C. M., Coughlin, M. L., Straight, A. F., and Mitchison, T. J. (2002) *Dev. Cell* **3,** 791–802
25. Macara, I. G., Baldarelli, R., Field, C. M., Glotzer, M., Hayashi, Y., Hsu, S. H., Kennedy, M. B., Kinoshita, M., Longtine, M., Low, C., Maltais, L. J., McKenzie, L., Mitchison, T. J., Nishikawa, T., Noda, M., Petty, E. M., Peifer, M., Pringle, J. R., Robinson, P. J., Roth, D., Russell, S. E., Stuhlmann, H., Tanaka, M., Tanaka, T., Trimble, W. S., Ware, J., Zeleznik-Le, N. J., and Zieger, B. (2002) *Mol. Biol. Cell* **13,** 4111–4113
26. Kinoshita, A., Noda, M., and Kinoshita, M. (2000) *J. Comp. Neurol.* **428,** 223–239
27. Kinoshita, A., Kinoshita, M., Akiyama, H., Tomimoto, H., Akiguchi, I., Kumar, S., Noda, M., and Kimura, J. (1998) *Am. J. Pathol.* **153,** 1551–1560
28. Larisch, S., Yi, Y., Lotan, R., Kerner, H., Eimerl, S., Tony Parks, W., Gottfried, Y., Birkey Reffey, S., de Caestecker, M. P., Danielpour, D., Book-Melamed, N., Timberg, R., Duckett, C. S., Lechleider, R. J., Steller, H., Orly, J., Kim, S. J., and Roberts, A. B. (2000) *Nat. Cell Biol.* **2,** 915–921
29. Zhang, Y., Gao, J., Chung, K. K., Huang, H., Dawson, V. L., and Dawson, T. M. (2000) *Proc. Natl. Acad. Sci. U. S. A.* **97,** 13354–13359
30. Chung, K. K., Dawson, V. L., and Dawson, T. M. (2001) *Trends Neurosci.* **24,** Suppl. 1, S7–S14
31. Gelb, D. J., Oliver, E., and Gilman, S. (1999) *Arch. Neurol.* **56,** 33–39
32. McKeith, I. G., Perry, E. K., and Perry, R. H. (1999) *Neurology* **53,** 902–905
33. Gilman, S., Low, P. A., Quinn, N., Albanese, A., Ben-Shlomo, Y., Fowler, C. J., Kaufmann, H., Klockgether, T., Lang, A. E., Lantos, P. L., Litvan, I., Mathias, C. J., Oliver, E., Robertson, D., Schatz, I., and Wenning, G. K. (1998) *J. Auton. Nerv. Syst.* **74,** 189–192
34. Mclean, P. J., Kawamata, H., and Hyman, B. T. (2001) *Neuroscience* **104,** 901–912
35. Zhang, J., Kong, C., Xie, H., McPherson, P. S., Grinstein, S., and Trimble, W. S. (1999) *Curr. Biol.* **9,** 1458–1467
36. Wakabayashi, K., Engelender, S., Tanaka, Y., Yoshimoto, M., Mori, F., Tsuji, S., Ross, C. A., and Takahashi, H. (2002) *Acta Neuropathol.* **103,** 209–214
37. Kato, K. (1990) *Eur. J. Neurosci.* **2,** 704–711
38. Takahashi, H., Ohama, E., Suzuki, S., Horikawa, Y., Ishikawa, A., Morita, T., Tsuji, S., and Ikuta, F. (1994) *Neurology* **44,** 437–441
39. Xu, J., Kao, S. Y., Lee, F. J., Song, W., Jin, L. W., and Yankner, B. A. (2002) *Nat. Med.* **8,** 600–606
40. Rideout, H. J., Larsen, K. E., Sulzer, D., and Stefanis, L. (2001) *J. Neurochem.* **78,** 899–908
41. Masliah, E., Rockenstein, E., Veinbergs, I., Sagara, Y., Mallory, M., Hashimoto, M., and Mucke, L. (2001) *Proc. Natl. Acad. Sci. U. S. A.* **98,** 12245–12250
42. Schlossmacher, M. G., Frosch, M. P., Gai, W. P., Medina, M., Sharma, N., Forno, L., Ochiishi, T., Shimura, H., Sharon, R., Hattori, N., Langston, J. W., Mizuno, Y., Hyman, B. T., Selkoe, D. J., and Kosik, K. S. (2002) *Am. J. Pathol.* **160,** 1655–1667
43. Gearing, M., Juncos, J. L., Procaccio, V., Gutekunst, C. A., Marino-Rodriguez, E. M., Gyure, K. A., Ono, S., Santoianni, R., Krawiecki, N. S., Wallace, D. C., and Wainer, B. H. (2002) *Ann. Neurol.* **52,** 465–476
44. Minamide, L. S., Striegl, A. M., Boyle, J. A., Meberg, P. J., and Bamburg, J. R. (2000) *Nat. Cell Biol.* **2,** 628–636
45. Perl, D. P., Olanow, C. W., and Calne, D. (1998) *Ann. Neurol.* **44,** Suppl. 1, S19–S31

EXHIBIT B

American Journal of Pathology, Vol. 153, No. 5, November 1998

Identification of Septins in Neurofibrillary Tangles in Alzheimer's Disease

Ayae Kinoshita,* Makoto Kinoshita,† Haruhiko Akiyama,§ Hidekazu Tomimoto,* Ichiro Akiguchi,* Sharad Kumar,¶ Makoto Noda,† and Jun Kimura*

From the Departments of Neurology and Molecular Oncology,† Kyoto University Graduate School of Medicine, Yoshida Konoe-cho, Sakyo-ku, Kyoto, Japan; the Department of Neuropathology,§ Tokyo Institute of Psychiatry, Tokyo, Japan; and the Hanson Centre for Cancer Research,¶ Institute of Medical and Veterinary Science, Adelaide, Australia*

Septins are evolutionarily conserved cytoskeletal GTPases that can form heteropolymer complexes involved in cytokinesis and other cellular processes. We detected expression of the human septin genes *Nedd5*, *H5*, *Diff6*, and *hCDC10* in postmortem brain tissues using the reverse transcription-coupled polymerase chain reaction and their products by immunoblot analysis. Four antibodies directed against three septins, Nedd5, H5, and Diff6, consistently labeled neurofibrillary tangles, neuropil threads, and dystrophic neurites in the senile plaques in brains affected by Alzheimer's disease but did not label obvious structures in young control brains. Immunoelectron microscopy revealed that Nedd5 localized to the paired helical filaments. Pre-tangles, the precursory granular deposits that accumulate in the neuronal cytoplasm, also were labeled with the antibodies. These findings suggest that at least the three septins are associated with tau-based paired helical filament core, and may contribute to the formation of neurofibrillary tangle as integral constituents of paired helical filaments. *(Am J Pathol 1998, 153:1551–1560)*

Alzheimer's disease (AD) is a group of neurodegenerative disorders of multiple pathogeneses. The histopathology of the AD brain is characterized by profound neuronal loss and two distinct pathological features: senile plaques and neurofibrillary changes including neurofibrillary tangles (NFTs), neuropil threads, and dystrophic neurites in the senile plaques.[1] The number of NFTs correlates with the severity of dementia,[2,3] indicating a positive role for NFT in the functional disturbance of tangled neurons. As exemplified by transgenic mice that overexpress one of the neurofilament subunits,[4,5] excessive cytoplasmic deposit of certain proteins can disturb neuronal homeostasis, resulting in acceleration of the degenerative processes. This may also be true with AD brains, in which NFTs progressively displace the normal neuronal cytoskeleton. Recent genetic approaches have revealed a number of key molecules for the pathogenesis of AD, ie, amyloid β-protein precursor (βPP), presenilins, and apolipoprotein E4.[6] So far, however, causal roles of these molecules in NFT formation have yet to be established.

NFT consists of a variety of abnormal filamentous structures represented by paired helical filaments (PHFs) 8–20 nm in diameter with a helical periodicity of 80 nm.[7] PHF is also the common structural basis of neuropil threads and a subset of dystrophic neurites in the senile plaque.[8] PHF is a heteropolymer complex of polypeptides, a major constituent of which is a microtubule-associated protein, tau. The presence of tau in NFT/PHF has been established by immunochemical analyses of brain tissues[9–11] and sequencing of PHF-derived peptides.[12–14] This structural heterogeneity of PHFs *in vivo* is attributable to biochemical modifications of tau[15–17] and/or involvement of other components.

Septins comprise a novel class of the GTPase family originally identified in the budding yeast mutants *CDC3*, *CDC10*, *CDC11*, and *CDC12*, which are commonly defective in cytokinesis.[18,19] The yeast septin gene products are the major constituents of the ~10-nm filaments formed beneath the plasma membrane at the mother-bud neck.[20,21] In *Drosophila*, at least three septins are concentrated near the contractile ring and in the nervous system as heteropolymer complexes.[22–24] In mammals, at least seven septin genes have been reported to date: *Diff6*,[25] *H5*,[26] and *Nedd5*[27,28] in the mouse and *hCDC10*,[29] KIAA0129, KIAA0158,[30] and *CDCrel-1*[31] in humans. Our database search and expression analyses revealed that (1) the counterparts of mouse *Diff6* and *H5* are expressed in humans, (2) the counterpart of *hCDC10* is expressed in the mouse, and (3) KIAA0158 is the human counterpart of the mouse *Nedd5* gene (see below). Thus the human and mouse genomes share at least four septin genes, *Diff6*, *H5*, *Nedd5*, and *CDC10*. (Note that the mammalian *CDC10* genes are not orthologs of the budding yeast *CDC10* gene.) We have been studying

Supported in part by Grants-in-Aid from the Ministry of Health and Welfare Brain Science Research Program (to MK) and the Ministry of Education, Science and Culture (to MK and MN) of Japan.

Accepted for publication August 5, 1998.

Address reprint requests to Dr. Makoto Kinoshita, Department of Molecular Oncology, Kyoto University Graduate School of Medicine, Yoshida Konoe-cho, Sakyo-ku, Kyoto 606-8501, Japan. E-mail: mkinoshi@virus.kyoto-u.ac.jp.

the mammalian septin system since we isolated the mouse *Nedd5* gene. Nedd5 is a ubiquitous cytoskeletal component that interacts with actin-based structures such as contractile ring and stress fibers.[28] Recently, a set of septins were identified in a protein complex that can interact with sec6/8 complex in the rat brain.[32] Since sec6/8 complex is a cluster of molecules essential for exocytosis, another role of the septins may be to link the secretory machinery to actin-based cytoskeleton beneath plasma membrane.

In the course of screening neuropathological implications of septins based on their potential to form a filamentous complex, we tested whether they can contribute to the neurofibrillary pathology. We report here that three human septins, Nedd5, Diff6, and H5, are commonly deposited in and around NFTs in AD brains, whereas hCDC10 is not. Our findings raise the possibility that at least three septins are involved in the neurodegeneration of AD by forming heteropolymer complexes which directly or indirectly interact with tau in the PHF.

Materials and Methods

Cases

Human brain tissue samples were obtained from the Department of Neurology, Kyoto University Hospital. Neuropathological diagnoses were based on the standard criteria for AD.[33] Tissues from age-matched patients without dementia-causing diseases were used as the controls. Three AD (range, 65–82 years) and 7 control (5 age-matched, range, 63–85 years; 2 young, 33 and 35 years) brain samples were analyzed by immunoblotting and reverse transcription-coupled polymerase chain reaction (RT-PCR), and five additional AD samples (range, 73–80 years) were used only for immunocytochemistry. Specimens taken from the right temporal cortices and hippocampi were quickly frozen in liquid nitrogen and then used in the biochemical analyses. Those taken from the left hemispheres were immersion-fixed and used in the histochemical analyses.

RNA Extraction and RT-PCR

The methods have been described elsewhere.[34] In brief, the poly(A)$^+$ RNA (1 μg) isolated from each hippocampal sample was reverse transcribed from an oligo-dT primer in 33 μl of reaction medium using First Strand Synthesis Kit (Pharmacia, Uppsala, Sweden). Each sample was diluted to 1000 μl and heat-inactivated, then 10 μl was amplified in a 20-μl standard PCR reaction mixture containing 0.2 μmol/L primers (see below) and 1.25 μCi [α-^{32}P]dCTP under the following conditions for 20 cycles: 0.5 minute at 96°C, 0.5 minute at 52°C, and 1 minute at 72°C. Each sample was electrophoresed through a 5% polyacrylamide gel and densitometry was done with an image analyzing system, BAS2000 (Fuji, Tokyo, Japan). The amount of amplified β-actin gene fragment was used to estimate the amount of input cDNA for calibration. Control experiments were performed to determine the range of PCR cycles over which amplification efficiency remained constant and to confirm that the amount of PCR product was proportional to the amount of input RNA. The identity of each PCR product was confirmed by its size and by direct sequencing. The following pairs of oligonucleotides were used as the primers (the corresponding nucleotide positions are shown in parentheses): KIAA0158/human *Nedd5*, AATCTGAGGATGAGACAGGG (2850–2869) and TGGGTAGTAAAACCAAAGGG (3258–3277); R53785/human *Diff6*, AAGCTTTCCCGCCAGAGCGC (3–22) and CGGGACGTGGCCTCAGAGGG (172–191); W69298/human *H5*, TCTCTGGGCAGTCAGCAGGG (31–50) and CATTATGGAGAACTACCGGG (379–398) S72008/*hCDC10*, CAAAGGTTCCATTCAGTGCAGC (1720–1741) and CTCTTCAAGAGGCCATGATTCC (2191–2212); X00351/human β-actin, AGAAGAGCTATGAGCTGCCTGACG (751–774) and TACTTGCGCTCAGGAGGAGCAATG (1028–1051).

Production and Purification of Antibodies

The production and characterization of the two anti-Nedd5 antibodies, 6 and 11, were reported previously.[28] We also raised antibodies against three synthetic peptides; C10C (EQQNSSRTLEKNKKKGKIF; residues 400–418 of hCDC10), H5C (DFPIPAVPPGTDPE; residues in the putative product of a human cDNA clone W69298 and mouse H5) and D6C (TEIPLPMLPLADTE, residues corresponding to a part of the putative product of a human cDNA clone R53785, which is similar to residues 315–328 of mouse Diff6). Each peptide was conjugated to an equal weight of maleimide-activated bovine serum albumin (Pierce, Rockford, Illinois) via a cysteine residue added to the amino-terminus. Animals were immunized with the bovine serum albumin-conjugated antigen (0.1 mg of H5C and C10C for a guinea pig, 0.5 mg of D6C for a rabbit) emulsified in Freund's complete adjuvant (Sigma, St. Louis, MO). After boosting with Freund's incomplete adjuvant (Sigma) once or twice, collected sera were fractionated with ammonium sulfate and affinity purified using the corresponding peptides coupled with fluoromethylpyridinium toluene sulfonate-activated Cellurofine (Seikagaku, Tokyo, Japan).

Immunoblot Analysis

We followed the standard protocols of Sambrook et al[35] with some modifications.[28] In brief, the frozen tissue samples were sonicated directly in nonreducing sodium dodecyl sulfate (SDS) buffer and then ultracentrifuged at 80,000 × *g* for 20 minutes. The supernatant was incubated at 100°C for 5 minutes with 2-mercaptoethanol. The lysate containing 25 μg of total protein was separated on 10% SDS-PAGE and transferred to a polyvinylide difluoride membrane (Micron Separations, Westborough, MA). The membrane was incubated overnight in the blocking buffer [0.2% Tween 20 in Tris-buffered saline (TBS, pH 7.4) containing 1% bovine serum albumin], then with each antibody (1 μg/ml) in the blocking buffer for 1 hour. The membrane was washed with TBS-

Tween 20 and then incubated in the blocking buffer containing an appropriate secondary antibody conjugated with alkaline phosphatase (Chemicon, Temecula, CA, 1:5000). The immune complex was detected by a chromogenic reaction. The signals were digitized with an optical scanner, GT8000 (Epson, Tokyo, Japan), and the software NIH Image 1.55 was used for densitometry.

Immunocytochemistry

We performed immunocytochemistry on the brain sections using rabbit polyclonal antibodies against Nedd5 (6 and 11) and Diff6 (D6C-1) and guinea pig polyclonal antibodies against H5 (H5C-1) and hCDC10 (C10C-1). Postmortem brain samples were immersion-fixed with 4% paraformaldehyde in 0.1 mol/L phosphate buffer (PB) for 24–48 hours. After cryoprotection for 48 hours h in 20% sucrose in 0.1 mol/L PB, the tissues were sliced 30 μm thick. The sections were treated for 0.5 hours with 0.5% H_2O_2 in 0.1 mol/L phosphate-buffered saline (PBS, pH 7.4) containing 0.1% Triton X-100 to deplete endogenous peroxidase activities. The slides were then incubated with the primary antibodies (1 μg/ml) followed by biotinylated anti-rabbit IgG (Vector, Burlingame CA, 1:200) or anti-guinea pig IgG (Vector, 1:200), and the avidin-biotin-horseradish peroxidase (Vector, 1:100). The specific immune complex was detected with diaminobenzidine-nickel ammonium sulfate.

For double immunofluorescence cytochemistry of H5 (H5C-1) and either Nedd5 (antibody 6) or Diff6 (D6C-1), the sections from AD brains were incubated with each combination of the primary antibodies, then with fluorescein isothiocyanate-conjugated anti-rabbit IgG antibody (Chemicon, 10 μg/ml) and biotinylated anti-guinea pig IgG antibody (Vector, 1:200), followed by treatment with Texas Red-conjugated avidin (Vector, 1:1000). For double staining of phosphorylated tau (Tau2, Sigma, 1:1000 or AT8, Innogenetics, Zwijndrecht, Belgium, 1:1000) and either of Nedd5 (6), H5 (H5C-1) or Diff6 (D6C-1), we used fluorescein isothiocyanate-conjugated anti-mouse IgG (Chemicon, 10 μg/ml) and biotinylated antibodies (ie, anti-rabbit IgG for Nedd5 and Diff6, and anti-guinea pig IgG for H5, Vector, 1:200) with Texas Red-conjugated avidin (Vector, 1:1000). The sections were observed through the appropriate filters.

Double staining for C4d and septins were done as follows: Sections were sequentially incubated with mouse monoclonal antibody against C4d (Quidel, San Diego, CA, 1:1000) and the biotinylated secondary antibody and developed for 10 minutes in a solution containing 0.02% diaminobenzidine and 150 μmol/L H_2O_2 in 50 mmol/L Tris-Cl (pH 7.6). After incubation in 150 mmol/L H_2O_2 in PBS for 30 minutes, the sections went through the second staining cycle with each of the anti-septin antibodies and biotinylated secondary antibody, then they were developed in 0.02% diaminobenzidine and 0.6% nickel ammonium sulfate solution. Consequently, C4d was stained brown and septins were labeled dark purple.

Immunoelectron Microscopy

A pre-embedding method was used for the immunoelectron microscopy. Paraformaldehyde-fixed entorhinal cortices from AD patients were sectioned (50 μm thick) in a vibratome. The sections were blocked with 20% normal goat serum for 1 hour and then incubated with anti-Nedd5 antibodies (6 or 11, 1 μg/ml) in 0.1 mol/L PB overnight at 4°C, followed by incubation with 1.4 nm gold-coupled anti-rabbit IgG (Nanoprobes, Stony Brook, NY, 1:100). Sections were postfixed in 1% glutaraldehyde in distilled water for 10 minutes. The sections were treated with HQ Silver enhancement kit (Nanoprobes), then with 1% OsO_4 in 0.1 mol/L PB, stained with 1% uranyl acetate, dehydrated in ethanol, and flat-embedded in epoxy resin. Serial ultrathin sections 50 nm thick were observed with an H-7100 electron microscope (Hitachi, Tokyo, Japan).

Results

Expression of Human Septin Genes in the Brain

The complete human septin cDNA sequences of KIAA0158 (encoding the human counterpart of mouse Nedd5, which we call human Nedd5 in this paper) and *hCDC10* are available in the database. In addition, there are partial human cDNA sequences (eg, accession nos. R36763 and W69298) encoding polypeptides that are 85% and 94% identical to the amino- and carboxy-terminal sequences, respectively, of mouse H5. Likewise, we found several other human cDNAs (eg, accession nos. AA262134 and R53785) encoding polypeptides that are 96% and 98% identical to the middle and carboxy-terminal portions, respectively, of mouse Diff6. Given the high interspecies conservation of the amino acid sequences of the septin counterparts (eg, 99% between human and mouse Nedd5) and the moderate amino acid identities (50–60%) shared among the septins in a given mammalian species,[18] these cDNA fragments are likely to be derived from the human counterparts of the mouse *H5* and *Diff6* genes. In this study, we have therefore regarded R36763/W69298 and AA262134/R53785 as partial cDNA fragments of the human *H5* and *Diff6* genes, respectively.

We assessed expression of the four human septin genes (*Nedd5*, *hCDC10*, *H5*, and *Diff6*) in postmortem brain samples using RT-PCR analysis. We found that the four septin genes were expressed in all of the brain samples investigated in this study: AD (n = 3), age-matched control (n = 5), and young control (n = 2) brains (Figure 1a). The identity of each PCR product was confirmed by size and DNA sequence. Densitometric data of each septin gene's expression level in the three groups were as follows (standardized with the β-actin gene expression level, arbitrary unit): *Nedd5* (AD 101 ± 7, age-matched 106 ± 12, young 119 ± 11), *hCDC10* (108 ± 3, 119 ± 8, 146 ± 16), *H5* (122 ± 5, 107 ± 4, 121 ± 1), *Diff6* (130 ± 2, 125 ± 4, 135 ± 16). We could not detect any consistent differences in the expression levels among these limited number of samples.

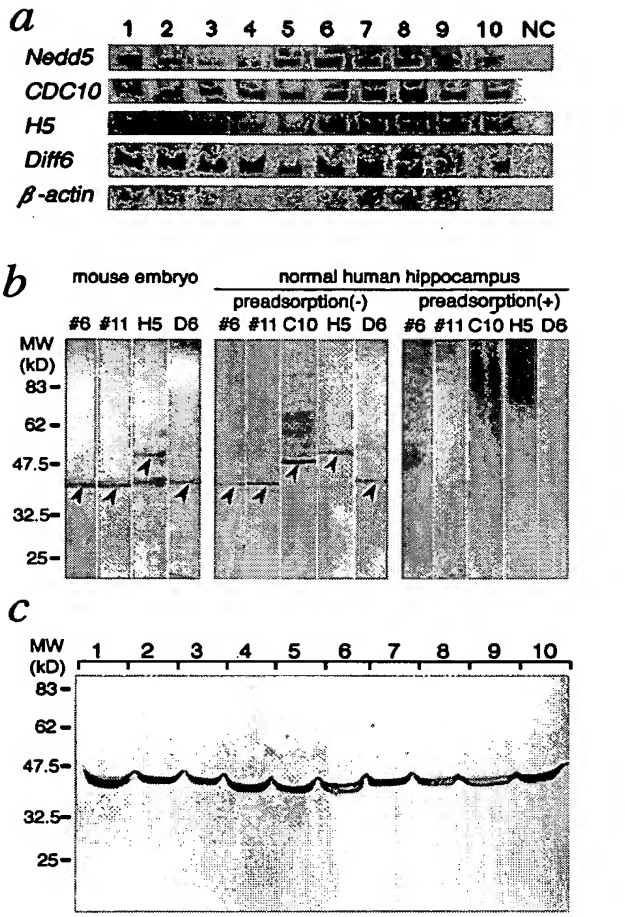

Figure 1. Expression of the four septins in AD and control brains. a: RT-PCR analysis of the human septin genes expressed in the hippocampus. Poly(A)$^+$ RNA (~10 ng) from human hippocampal regions was reverse-transcribed and subjected to PCR using primer sets for human Nedd5, Diff6, H5, and hCDC10, and for β-actin as an internal control. Representative results for AD brains (lanes 1–3), age-matched (lanes 4–7, 10) and young (lanes 8, 9) control brains, and a negative control without template cDNA (NC) are shown. b: Characterization of the four anti-septin antibodies used in this study. Each antibody (6 and 11 for Nedd5, H5C-1 for H5, and D6C-1 for Diff6) was tested by immunoblotting of lysates from mouse embryos (at gestational day 13.5) and a normal human hippocampus. Each lane contained 25 μg of total protein. Immunoreactive bands (arrowheads) were abolished when antibodies preadsorbed with the corresponding antigens were used. c: Immunoblot of the hippocampal lysates of AD and control brains. A representative blot showing Nedd5 (detected by antibody 11) in brains from AD patients (lanes 1–3), age-matched controls (lanes 4–7, 10) and the young individuals (lanes 8, 9). Each lane contained 25 μg of total protein.

Characterization of the Septin Antibodies

We raised polyclonal antibodies against the four mammalian septins (Nedd5, H5, Diff6 and CDC10) using recombinant proteins or synthetic peptides that correspond to amino acid sequences highly conserved between the human and mouse counterparts but distinct from the other septins. Authenticity of the two antibodies (6 and 11) that recognize distinct regions of human/mouse Nedd5 was established previously.[28] Three other antibodies were raised against synthetic peptides corresponding to portions near the carboxy-termini of H5, Diff6, and CDC10 (H5C-1, D6C-1, C10C-1), respectively. These sequences were not shared by any other polypeptide in the database.

Using these antibodies, we performed immunoblot analysis with mouse embryonic and human brain tissues. As we reported previously,[28] the two anti-Nedd5 antibodies detected 41.5-kd proteins both in the mouse and human tissues. These bands were abolished after treatment of each antibody with excess corresponding antigen (Figure 1b). Likewise, each of the antibodies H5C-1, D6C-1, and C10C-1 detected a single band of expected size (54, 42, and 49 kd, respectively) in the human and mouse tissue samples (Figure 1b). Each band was abolished by preadsorption with excess amount of the corresponding antigen but not with the other septin antigens (Figure 1b and data not shown). These results established that each antibody reacted specifically with the corresponding human septins in the brain samples without mutual cross-reactivity. The molecular weights of the putative human H5, Diff6 and hCDC10 estimated by the immunoblotting are comparable to those of the mouse homologs, providing additional evidence of their identity as the human counterparts.

We assessed the amount of Nedd5 in SDS-soluble fractions of the hippocampal and temporal cortices from AD (n = 3), age-matched control (n = 5), and young control (n = 2) brains. Densitometric analysis of the bands showed no consistent differences among the groups; AD 116 ± 16, age-matched 145 ± 20, young 136 ± 13 (Figure 1c).

Detection of Septins in Brain Tissue Sections

We immunostained paraformaldehyde-fixed, free-floating tissue sections from histopathologically confirmed AD brains (n = 8) as well as from those of age-matched (n = 5) and young (n = 2) control cases. Anti-Nedd5 antibody 6 labeled numerous NFTs and neuropil threads in the entorhinal cortex of AD brains (Figure 2a). Positive staining was completely abolished by preadsorption of the antibodies with excess antigens but was not affected by preadsorption with antigens of the other septins (Figure 2, a and b, and data not shown). Elimination of the primary antibodies also abolished the signals. In contrast, these antibodies did not label obvious structures more than diffuse cytoplasmic staining in the young control brains (Figure 2c and data not shown). In AD brains, antibodies 6 and 11 against Nedd5 consistently stained NFTs (Figure 2, d and e). Nedd5 was also detected in neurites in the neuropil (neuropil threads) and dystrophic neurites in senile plaques of AD brains (Figure 2a). These Nedd5-positive structures were abundant, particularly in the hippocampus and entorhinal cortex. Antibodies against H5 (H5C-1) and Diff6 (D6C-1) gave essentially the same staining patterns as those of 6 and 11, whereas an antibody against hCDC10 (C10C-1) did not label NFTs (Figure 2, f and g, and data not shown). NFTs sparsely distributed in the age-matched entorhinal cortices were

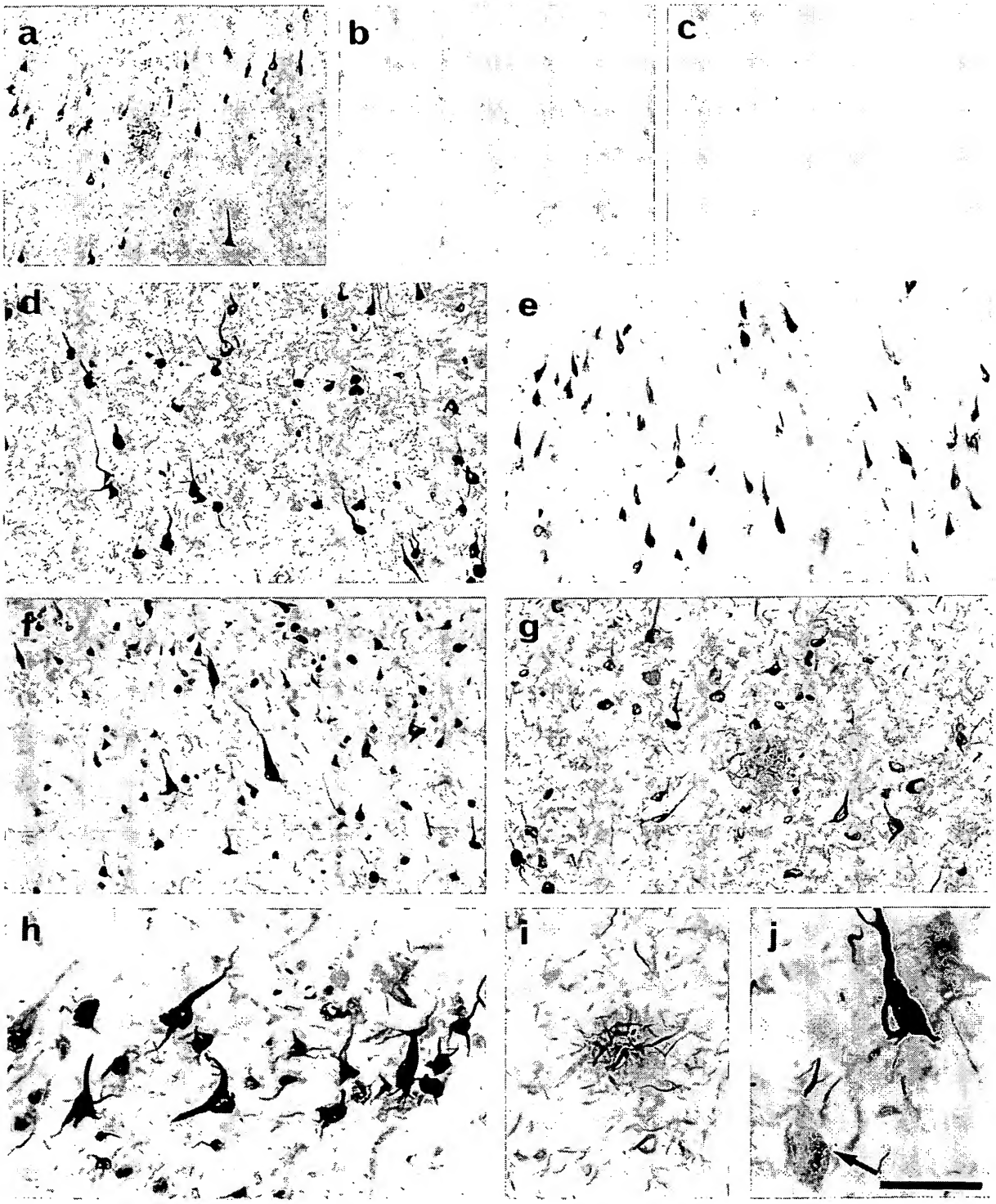

Figure 2. Immunocytochemical detection of septins in AD and control brains. a: Anti-Nedd5 antibody 6 labeled numerous NFTs, neuropil threads and dystrophic neurites in the senile plaques in the entorhinal cortex of an AD brain. b: Preadsorption of 6 with the antigen peptide abolished the signals on an adjacent section from the same patient as in a. c: A representative section of the entorhinal cortex from a young individual showing minimal cytoplasmic staining for Nedd5. d to g: Sections of the entorhinal cortex and hippocampus from AD brains immunostained with the following anti-septin antibodies; 6 (d) and 11 (e) for Nedd5, H5C-1(f) for H5, and D6C-1(g) for Diff6. NFTs, neuropil threads, and dystrophic neurites are intensely labeled with the four antibodies but the normal-appearing neurons are not stained. h to j: Higher magnifications of the immunolabeled AD brain sections. NFTs, neuropil threads (h), and dystrophic neurites of senile plaque (i) are intensely stained with anti-Nedd5 antibody 6. Some glial tangles are also seen in h. In j, H5-immunoreactive granules (pre-tangles) beside the manifest NFT in the neuronal cytoplasm are shown (arrow). Scale: 200 μm (a-c), 130 μm (d, e) , 100 μm (f, g), 50 μm (h-j).

also stained for Nedd5, H5, and Diff6, but not for hCDC10 (data not shown).

The three septins (Nedd5, H5 and Diff6) were also detected in the cytoplasm of a small number of neurons that did not manifest NFTs, where immunoreactivities were distributed in a granular pattern (Figure 2j and data not shown), probably corresponding to the pre-tangles (also referred to as stage 0 tangles[36] or Group 1 tangles[37]).

Septin-positive fibrous structures, which appear to be glial tangles in astrocytes, were also found in small non-pyramidal cells in AD brains (Figure 2h).

Colocalization of Septins and Tau in Intracellular NFTs

Drosophila and rat septins are known to form heteropolymer complexes *in vivo*.[23,24,32] However, we found that tissue distribution and subcellular localization of Nedd5, H5, Diff6, and CDC10 in mouse and human cells are not necessarily identical (Kinoshita, Valencik, Kinoshita, Pringle, and Noda, manuscript in preparation). Thus we tested colocalization of the septins in NFTs. Double immunofluorescence staining of the hippocampus and entorhinal cortex of AD brains showed largely overlapping labeling patterns for H5 and Diff6 (Figure 3, a and b), except for a few Diff6-positive NFTs that were H5-negative (arrowheads in Figure 3b). Similar results were obtained for the combination of Nedd5 and H5 (data not shown). We then compared localization of the septins and tau, the major constituent of NFTs. For instance, double labeling of AD hippocampi for Diff6 (with D6C-1 antibody) and phosphorylated tau (with commercial antibodies Tau2 or AT8) showed that roughly 95% of NFTs were doubly labeled for both tau and Diff6 (Figure 3, c and d). We therefore concluded that the septins localize close to the phosphorylated tau in the majority of NFTs. Interestingly, however, some other neurons appeared to contain almost exclusively either tau (Figure 3f) or Diff6 (Figure 3e). Even in the double-positive neurons, subcellular distributions of Diff6 and tau appear overlapping but not identical (Figure 3, c and d): tau is enriched both in somatic and dendritic NFTs, whereas Diff6 appears to localize more proximally (see Discussion). These data also support the observation that the antibodies are not mutually cross-reactive.

After disintegration of tangled neurons, NFTs are known to remain *in situ* and exposed to the extracellular milieu. These extracellular NFTs (eNFTs) have a unique immunocytochemical profile: ie, a number of tau epitopes have been lost, probably through proteolytic processing. Meanwhile, activation of the complement system takes place against eNFTs, resulting in heavy decoration with various complement proteins.[38] Our double-staining analysis showed that the distribution patterns of septin-positive NFTs and complement C4d-positive NFTs (eNFTs) were mutually exclusive (Figure 3g). These findings indicate that septin-positive NFTs are formed intracellularly and that the septin epitopes may be lost due to proteolytic degradation or other modifications after neuronal collapse.

Electron Microscopic Detection of a Septin in PHF

Ultrastructural localization of a septin in the NFTs was analyzed in the entorhinal cortex of AD patients using a pre-embedding, immunogold-labeling method by using anti-Nedd5 antibodies (6 and 11). Both of the two antibodies gave specific labeling along PHFs (Figure 4, a and b, and data not shown). No labeling was detected in association with neurofilaments, glial fibrils or any other normal structures in the cytoplasm.

Discussion

We showed that the three human septins, Nedd5, H5 and Diff6, are concentrated in intracellular NFTs, dystrophic neurites in senile plaques, neuropil threads in the brains of all of the AD patients studied and, to a much lesser extent, in some elderly controls. It is unlikely that staining was due to nonspecific labeling or cross-reactivity to other proteins, in particular the major NFT component tau, for three reasons: (1) none of the known septins shares similarities in the primary structure with tau; (2) the results were consistent with antibodies directed against two distinct epitopes in Nedd5; and (3) double staining with each septin and tau revealed a minor but obvious dissociation in their localization.

As assessed by the RT-PCR and immunoblot analyses, brains from young individuals contain as much septin mRNAs and their products as AD brains. By immunocytochemistry, however, no obvious structure more than diffuse cytoplasmic staining was found in young brains (Figure 2b). We are not sure of the specificity of this staining because the signal intensity is as weak as the background level of preadsorbed one (Figure 2c). Such discrepancy between the immunoblot and immunocytochemistry results is reminiscent of the case of tau.[39] In normal neurons, tau is distributed along microtubules or diffusely in the cytoplasm, which is barely detectable with current immunocytochemical techniques. Tau becomes detectable only at high concentrations in the neurofibrillary changes. Similar explanation may apply to the septins. In addition, certain conformational changes through the aggregation process might enhance immunoreactivity, as has been proposed for anti-tau antibodies, Alz-50 and MC-1.[40] Our negative results with an anti-hCDC10 antibody could be explained by reduced immunoreactivity after conformational changes or epitope masking through complex formation. Alternatively, hCDC10 may be in fact excluded from NFT because isoelectric points of Nedd5, Diff6, and H5 are 6.2, 5.6, and 5.5, respectively, whereas those of hCDC10 and tau are 9.0 and 9.9. Thus, the three acidic septins can be highly interactive with extremely basic protein tau, while a basic septin hCDC10 cannot.

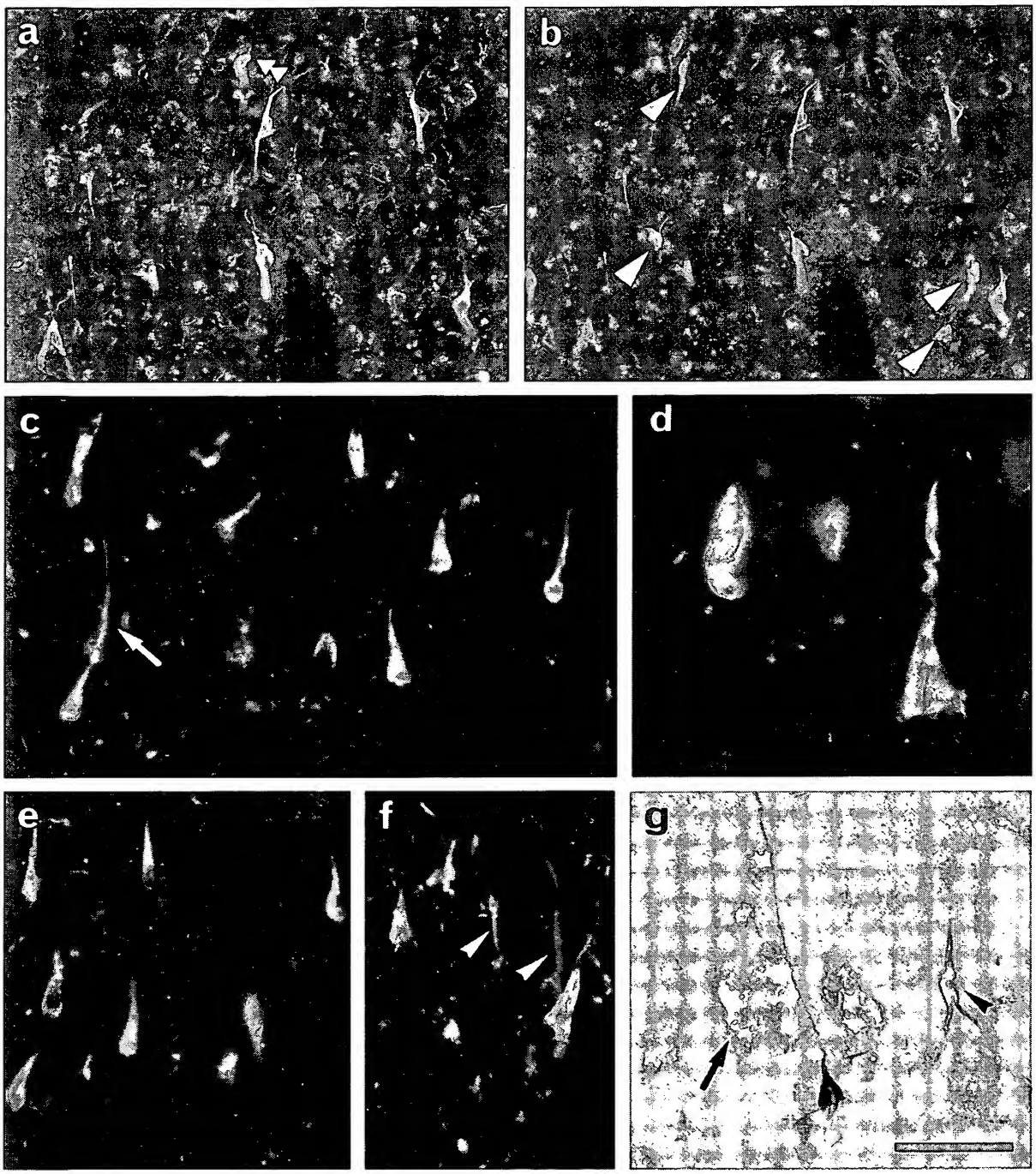

Figure 3. Double immunolabeling analyses of the entorhinal cortices from AD brains. a and b: H5 (a) and Diff6 (b) were labeled respectively with Texas Red and fluorescein. Signals for H5 and Diff6 largely overlap in the NFTs. However, a few NFTs are positive exclusively for H5 (double arrowhead) or Diff6 (arrowheads). c–f: Tau and Diff6 were labeled respectively with fluorescein (green) and Texas Red (red). The two signals were largely colocalized (shown as yellow in c, d), but found dissociated in some cases; ie, red cells (e) and green cells (f) (arrowheads). Note their distinct subcellular distribution in a single neuron (arrow in c, d). g: C4d and Nedd5 (6) were labeled brown and dark purple, respectively. Note that C4d-positive extracellular NFTs contain little, if any, immunoreactivity for Nedd5 (arrowhead). Diffuse plaques are intensely stained for C4d but not for Nedd5 (arrow). Scale: 100 μm.

The three septins exist not only in typical NFTs but in granular or fine fibrillar deposits in the neuronal soma as well. These structures may be considered as the earliest detectable stage of NFT formation (stage 0 tangles[36] or Group 1 tangles[37]). These changes were not found in young control brains, but were sparsely present in elderly controls. This may reflect the fact that degenerative neuronal changes accompanied by NFTs also develop, to a

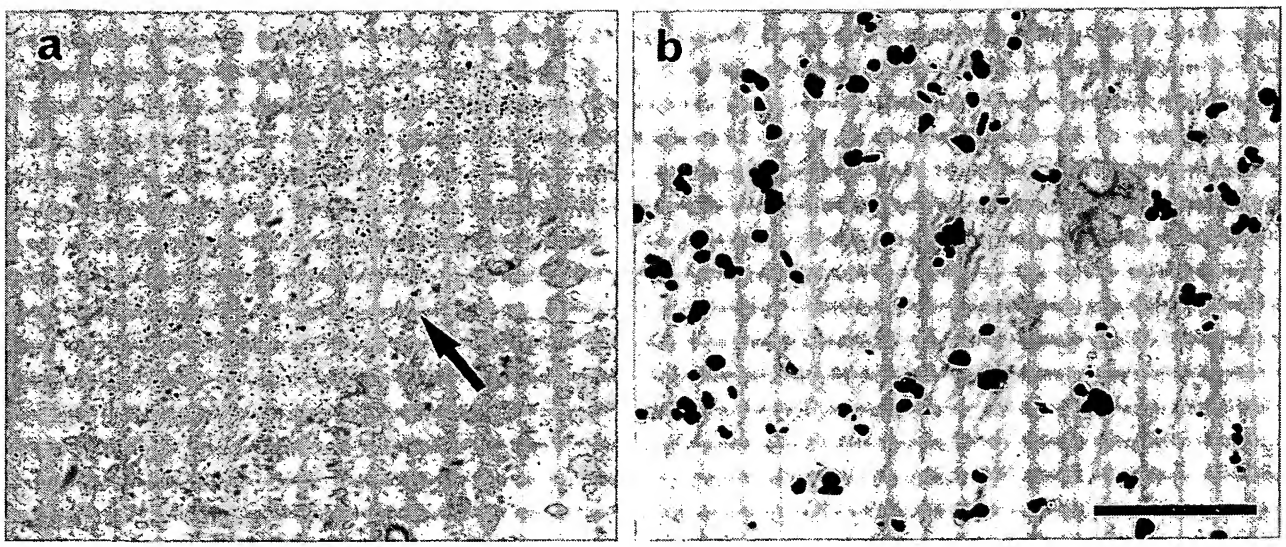

Figure 4. Immunoelectron micrographs for Nedd5 in the entorhinal cortex of an AD brain. a: An electron micrograph showing that gold particles for Nedd5 (arrow) specifically labeled NFTs in the neuronal cytoplasm. Scale: 4 μm. b: A higher magnification of the NFTs. The gold particles are concentrated along PHFs in the cytoplasm. Scale: 0.4 μm.

much lesser extent, with normal aging.[41] The presence of septins in such pre-tangles indicates that precursory, septin-containing aggregates are formed diffusely in the cytoplasm during the latent or earliest stage of NFT formation. The dissociation of immunoreactivities for septins and tau in a minor fraction of tangled neurons (Figure 3, e and f) may be attributable to masking of the epitopes by steric hindrance or secondary modification. However, the composition of Diff6-positive, phosphorylated tau-negative NFT-like structures (Figure 3e) would be intriguing because such accumulation of septins might be a novel mode of neurodegeneration.

Ample evidence has established that hyperphosphorylated tau is the major constituent of PHFs.[15] Because hyperphosphorylation of tau reduces its affinity for microtubules, it has been postulated that the increased unbound tau in the cytoplasm aggregates into PHFs. However, failure of tau-overexpressing transgenic mice to develop neurofibrillary changes[42] suggests that additional factors are required to promote NFT/PHF formation. On the other hand, extracellular accumulation of amyloid β protein (Aβ) is considered as a major factor in AD, but transgenic mice that overexpress βPP or its variants do not develop NFTs despite heavy Aβ deposits in the brain.[43,44] Such diseases as dementia pugilistica, viral encephalitis (subacute sclerosing panencephalitis), Guam Parkinson-dementia complex,[45] Niemann-Pick disease type C,[46] and myotonic dystrophy[47] show neurofibrillary pathology without marked Aβ deposits. These data indicate that diverse factors can trigger NFT formation as a final common pathway; however, tau is not sufficient and Aβ deposition is not necessary.

We have demonstrated that Nedd5, hCDC10, H5, and Diff6 are associated with actin cytoskeleton and recruited in the neurite and growth cone[28] (Kinoshita, Valencik, Kinoshita, Pringle, and Noda, manuscript in preparation). Recently, a fraction of septins in the cytoplasm have been identified in a complex that interacts with the sec6/8 complex in the rat brain.[32] Although physiological functions of the septin complex in the mammalian brain are yet to be determined, these and other data obtained in other species[18,21,23] suggest that mammalian septins provide scaffolds for organization of submembranous structures, neuronal polarity, and vesicle trafficking. We have previously shown that the assembly of septin filament is regulated by several factors such as growth signals, actin filament, and GTP hydrolysis, and that direct and indirect disturbances of these factors result in abnormal distribution and aggregation of Nedd5.[28] Therefore, whatever the original pathogenetic factors may be, disturbed septin assembly in neurons may affect the vesicular transport and structural integrity, eventually accelerating the degenerative processes.

Septins are also present in glial tangles in some degenerating astrocytes (Figure 2h). We also observed septin-positive glial tangles in the brains of multiple system atrophy patients (unpublished data). Thus involvement of septins in the pathological structures may be a common degenerative process in neuronal and glial lineages across distinct disease entities.

We found that overexpression of *Nedd5* in cultured cells gives rise to septin-containing fibrous or flame-shaped deposits in the cytoplasm (unpublished data). This suggests that excessive and/or disproportional aggregation of septin monomers in the cytoplasm can provide scaffolds for further recruitment of proteins such as septins and tau, promoting formation of pre-tangles and, subsequently, of NFTs. Testing whether the septin scaffolds accelerate the organization of tau into NFTs, or vice versa, should provide important insights into the molec-

ular mechanisms of NFT formation and the neuronal defects in AD.

Acknowledgments

We thank Ms. M. Fukuda, K. Imai, and A. Miyazaki for technical and/or secretarial assistance.

References

1. Yankner BA, Mesulam MM: Seminars in medicine of the Beth Israel Hospital, Boston. Beta-amyloid and the pathogenesis of Alzheimer's disease. N Engl J Med 1991, 325:1849–1857
2. McKee AC, Kosik KS, Kowall NW: Neuritic pathology and dementia in Alzheimer's disease. Ann Neurol 1991, 30:156–165
3. Arriagada PV, Growdon JH, Hedley-White T, Hyman BT: Neurofibrillary tangles but not senile plaques parallel duration and severity of Alzhemier's disease. Neurology 1992, 42:631–639
4. Xu Z, Cork LC, Griffin JW, Cleveland DW: Increased expression of neurofilament subunit NF-L produces morphological alterations that resemble the pathology of human motor neuron disease. Cell 1993, 73:23–33
5. Côté F, Collard J-F, Julien J-P: Progressive neuropathy in transgenic mice expressing the human neurofilament heavy gene: a mouse model of amyotrophic lateral sclerosis. Cell 1993, 73:35–46
6. Yankner BA: New clues to Alzheimer's disease: Unraveling the roles of amyloid and tau. Nature Med 1996, 2:850–852
7. Kidd M: Paired helical filaments in electron microscopy of Alzheimer's disease. Nature 1963, 197:192–193
8. Braak H, Braak E, Grundke-Iqbal I, Iqbal K: Occurrence of neuropil threads in the senile human brain and in Alzheimer's disease: a third location of paired helical filaments outside of neurofibrillary tangles and neuritic plaques. Neurosci Lett 1986, 65:351–355
9. Grundke-Iqbal I, Iqbal K, Quinlan M, Tung Y-C, Zaidi MS, Wisniewski HM: Microtubule-associated protein tau: a component of Alzheimer paired helical filaments. J Biol Chem 1986, 261:6084–6089
10. Kosik KS, Joachim CL, Selkoe DJ: The microtubule-associated protein tau is a major antigenic component of paired helical filaments in Alzheimer's disease. Proc Natl Acad Sci USA 1986, 83:4044–4048
11. Wood JG, Mirra SS, Pollock NJ, Binder LI: Neurofibrillary tangles of Alzheimer's disease share antigenic determinants with the axonal microtubule-associated protein tau. Proc Natl Acad Sci USA 1986, 83:4040–4043
12. Goedert M, Wischik CM, Crowther RA, Walker JE, Klug A: Cloning and sequencing of the cDNA encoding a core protein of the paired helical filament of Alzheimer's disease: identification as the microtubule-associated protein tau. Proc Natl Acad Sci USA 1988, 85:4051–4055
13. Kondo J, Honda T, Mori H, Hamada Y, Miura R, Ogawara M, Ihara Y: The carboxyl third of tau is tightly bound to paired helical filaments. Neuron 1988, 1:827–834
14. Wischik CM, Novak M, Thogersen HC, Edwards PC, Runswick MJ, Jakes R, Walker JE, Milstein C, Roth M, Klug A: Isolation of a fragment of tau derived from the core or the paired helical filament of Alzheimer's disease. Proc Natl Acad Sci USA 1988, 85:4506–4510
15. Morishima-Kawashima M, Hasegawa M, Takio K, Suzuki M, Yoshida H, Watanabe A, Titani K, Ihara Y: Hyperphosphorylation of tau in PHF. Neurobiol Aging 1995, 16:365–380
16. Mori H, Kondo J, Ihara Y: Ubiquitin is a component of paired helical filaments in Alzheimer's disease. Science 1987, 235:1641–1644
17. Wang J-H, Grundke-Iqbal I, Iqbal K: Glycosylation of microtubule-associated protein tau: An abnormal posttranslational modification in Alzheimer's disease. Nature Med 1996, 2:871–875
18. Longtine MS, DeMarini DJ, Valencik ML, Al Awar OS, Fares H, De-Virgilio C, Pringle JR: The septins: roles in cytokinesis and other processes. Curr Opin Cell Biol 1996, 8:106–119
19. Cooper JA, Kiehart DP: Septins may form a ubiquitous family of cytoskeletal filaments. J Cell Biol 1996, 134:1345–1348
20. Byers B: The molecular biology of the yeast *Saccharomyces*. Life Cycle and Inheritance. Edited by Strathern JN, Jones EW, Broach JR. Vol. 1. Cold Spring Harbor, NY, Cold Spring Harbor Laboratory Press, 1981, pp 59–96
21. Chant J: Septin scaffolds and cleavage planes in *Saccharomyces*. Cell 1996, 84:187–190
22. Neufeld TP, Rubin GM: The *Drosophila* peanut gene is required for cytokinesis and encodes a protein similar to yeast putative bud neck filament proteins. Cell 1994, 77:371–379
23. Fares H, Peifer M, Pringle JR: Localization and possible functions of *Drosophila* septins. Mol Biol Cell 1995, 6:1843–1859
24. Field CM, Al-Awar O, Rosenblatt ML, Alberts BM, Mitchison TJ: A purified *Drosophila* septin complex forms filaments, and exhibits GTPase activity: J Cell Biol 1996, 133:605–616
25. Nottenburg C, Gallatin WM, St.John T: Lymphocyte HEV adhesion variants differ in the expression of multiple gene sequences. Gene 1990, 95:279–284
26. Kato K: A collection of cDNA clones with specific expression patterns in mouse brain. Eur J Neurosci 1990, 2:704–711
27. Kumar S, Tomooka Y, Noda M: Identification of a set of genes with developmentally down-regulated expression in the mouse brain. Biochem Biophys Res Commun 1992, 185:1155–1161
28. Kinoshita M, Kumar S, Mizoguchi A, Ide C, Kinoshita A, Haraguchi T, Hiraoka Y, Noda M: Nedd5, a mammalian septin, is a novel cytoskeletal component interacting with actin-based structures. Genes Dev 1997, 11:1535–1547
29. Nakatsuru S, Sudo K, Nakamura Y: Molecular cloning of a novel human cDNA homologous to CDC10 in *Saccharomyces cerevisiae*. Biochem Biophys Res Commun 1994, 202:82–87
30. Nagase T, Seki N, Tanaka A, Ishikawa K, Nomura N: Prediction of the coding sequences of unidentified human genes. IV. The coding sequences of 40 new genes (KIAA0121-KIAA0160) deduced by analysis of cDNA clones from human cell line KG-1. DNA Res 1995, 2:167–174
31. Zieger B, Hashimoto Y, Ware J: Alternative expression of platelet glycoprotein Ib(β) mRNA from an adjacent 5′ gene with an imperfect polyadenylation sequence. J Clin Invest 1997, 99:520–525
32. Hsu S-C, Hazuka CD, Roth R, Foletti DL, Heuser J, Scheller RH: Subunit composition, protein interaction and structures of the mammalian brain sec6/8 complex and septin filaments. Neuron 1998, 20:1111–1122
33. Mirra SS, Hart MN, Terry RD: Making the diagnosis of Alzheimer's disease. A primer for practicing pathologists. Arch Pathol Lab Med 1993, 117:132–144
34. Kinoshita M, Tomimoto H, Kinoshita A, Kumar S, Noda M: Up-regulation of the *Nedd2* gene encoding an ICE/Ced-3-like cysteine protease in the gerbil brain after transient global ischemia. J Cereb Blood Flow Metab 1997, 17:507–514
35. Sambrook J, Fritsch EF, Maniatis T: Molecular Cloning: A Laboratory Manual (2nd ed.) Cold Spring Harbor, NY, Cold Spring Harbor Laboratory Press, 1989
36. Bancher C, Brunner C, Lassmann H, Budka H, Jellinger K, Wiche G, Seitelberger F, Grundke-Iqbal I, Iqbal K, Wisniewski HM: Accumulation of abnormally phosphorylated tau protein precedes the formation of neurofibrillary tangles in Alzheimer's disease. Brain Res 1989, 477:90–99
37. Braak E, Braak H, Mandelkow E-M: A sequence of cytoskeleton changes related to the formation of neurofibrillary tangles and neuropil threads. Acta Neuropathol 1994, 87:554–567
38. McGeer PL, Akiyama H, Itagaki S, McGeer EG: Immune system response in Alzheimer's disease. Can J Neurol Sci 1989, 16:516–527
39. Wolozin B, Davies P: Alzheimer-related neuronal protein A68: specificity and distribution. Ann Neurol 1987, 22:521–526
40. Jicha GA, Bowser R, Kazam IG, Davies P: Alz-50 and MC-1, a new monoclonal antibody raised to paired helical filaments, recognized conformational epitopes on recombinant tau. J Neurosci Res 1997, 48:128–132
41. Dickson DW, Crystal HA, Mattiace LA, Masur DM, Blau AD, Davies P, Yen SH, Aronson MK: Identification of normal and pathological aging in prospectively studied nondemented elderly humans. Neurobiol Aging 1992, 13:1–11
42. Götz J, Probst A, Spillantini MG, Schäfer T, Jakes R, Bürki K, Goedert M: Somatodendritic localization and hyperphosphorylation of tau protein in transgenic mice expressing the longest human brain tau isoform. EMBO J, 1995, 14:1304–1313
43. Games D, Adams D, Alessandrini R, Barbour R, Berthelette P, Black-

well C, Carr T, Clemens J, Donaldson T, Gillespie F, Guido T, Hagopian S, Johnson-Wood K, Khan K, Lee M, Leibowitz P, Lieberburg I, Little S, Masliah E, McConlogue L, Montoya-Zavala M, Mucke L, Paganini L, Penniman E, Power M, Schenk D, Seubert P, Snyder B, Soriano F, Tan H, Vitale J, Wadsworth S, Wolozin B, Zhao J: Alzheimer-type neuropathology in transgenic mice overexpressing V717F β-amyloid precursor protein. Nature 1995, 373:523–527

44. Hsiao K, Chapman P, Nilsen S, Eckman C, Harigaya Y, Younkin S, Yang F, Cole G: Correlative memory deficits, Aβ elevation and amyloid plaques in transgenic mice. Science 1996, 274:99–102
45. Wisniewski K, Jervis GA, Moretz RC, Wisniewski HM: Alzheimer neurofibrillary tangles in diseases other than senile and presenile dementia. Ann Neurol 1979, 5:288–294
46. Suzuki K, Parker CC, Pentchev PG, Katz D, Ghetti B, D'Agostino AN, Carstea ED: Neurofibrillary tangles in Niemann-Pick disease type C. Acta Neuropathol 1995, 89:227–238
47. Kiuchi A, Otsuka N, Namba Y, Nakano I, Tomonaga M: Presenile appearance of abundant Alzheimer's neurofibrillary tangles without senile plaques in the brain in myotonic dystrophy. Acta Neuropathol 1991, 82:1–5
48. Neve RL, Robakis NK: Alzheimer's disease: a re-examination of the amyloid hypothesis. Trends Neurosci 1998, 21:15–19

EXHIBIT C

lymphocytes. This indicates that the observed cytotoxicity depends on the integrity of the islet cell surface constituents.

Taken together, our results show that pancreatic expression of IFN-γ can result in immune sensitization of the transgenic mice to islets. In other experiments involving ectopic expression of antigens in islets, no islet immune-related destruction results, irrespective of whether tolerance is induced[9]. Indeed, there are other examples of T cells reactive to components in the periphery existing in a quiescent state[10–19]. *In vitro* experiments have demonstrated that IFN-γ can induce co-stimulatory activity leading to T cell activation[2,3], so when produced *in vivo*, it might activate quiescent autoreactive cells, stimulating lymphocytes to destroy both transgenic and normal islets. Our work implies that *in vivo* the lymphokine IFN-γ activates T cells so that they do not remain anergic to antigens encountered in the periphery. □

Received 9 April; accepted 14 June 1990.

1. Sarvetnick, N., Liggitt, D., Pitts, S. L., Hansen, S. E. & Stewart, T. A. *Cell* **52**, 773–782 (1988).
2. Hawrylowicz, C. M. & Unanue, E. R. *J. Immun.* **141**, 4083–4088 (1988).
3. Weaver, C. T., Hawrylowicz, C. M. & Unanue, E. R. *Proc. natn. Acad. Sci. U.S.A.* **85**, 8181–8185 (1988).
4. Bosma, G. C., Custer, R. P. & Bosma, M. J. *Nature* **301**, 527 (1983).
5. Duijvestijn, A. M., Schreiber, A. B. & Butcher, E. C. *Proc. natn. Acad. Sci. U.S.A.* **83**, 9114–9118 (1986).
6. Brown, J., Molnar, I. G., Clark, W. & Mullen, Y. *Science* **184**, 1377–1379 (1974).
7. Kemp, C. V., Knight, M. G., Scharp, D. W., Lacy, P. E. & Ballinger, W. F. *Nature* **244**, 447 (1973).
8. Campbell, I. L., Iscaro, A. & Harrison, L. C. *J. Immun.* **141**, 2325 (1988).
9. Harrison, L. C., Campbell, I. C., Allison, J. & Miller, J. F. A. P. *Diabetes* **38**, 815–818 (1989)
10. Mitchison, N. A. *Immunology* **15**, 509–530; 531–547 (1968).
11. Hooper, D. C., Young, J. L., Elson, C. J. & Taylor, R. B. *Cell. Immun.* **106**, 53–61 (1987).
12. Hooper, D. C. & Taylor, R. B. *Eur. J. Immun.* **17**, 797 (1987).
13. Rammensee, H. G., Kroschewski, R. & Frangoulis, B. *Nature* **339**, 541–544 (1989).
14. Qin, S., Cubbold, S., Benjamin, R. & Waldmann, H. *J. exp. Med.* **169**, 779–794 (1989).
15. Markmann, J. *et al. Nature* **336**, 476–479 (1988).
16. Burkly, L. C., Lo, D., kanagawa, O., Brinster, R. L. & Flavell, R. A. *Nature* **342**, 564–566 (1989).
17. Lo, D., Burkly, L. C., Flavell, R. A., Palmiter, R. D. & Brinster, R. L. *J. exp. Med.* **170**, 87–104 (1989).
18. Bohme, J. *et al. Science* **211**, 1179–1183 (1989).
19. Murphy, K. M., Weaver, C. T., Elish, M., Allen, P. M. & Loh, D. Y. *Proc. natn. Acad. Sci. U.S.A.* **86**, 10034–10038 (1989).

ACKNOWLEDGEMENTS. This work was supported by an MDA postdoctoral fellowship (N.S.), by a JDF postdoctoral fellowship (J.S.) and an NIH grant (J.S. and B.M.). T.G.P. is a scholar of the Leukemia Society of America. N.S. and J.S. thank Dr Garry Fathman for support.

Targeted disruption of the murine *int-1* proto-oncogene resulting in severe abnormalities in midbrain and cerebellar development

Kirk R. Thomas & Mario R. Capecchi*

Howard Hughes Medical Institute, Department of Biology and Human Genetics, Salt Lake City, Utah 84112, USA

THE *int-1* proto-oncogene was first identified as a gene activated in virally induced mouse mammary tumours[1,2]. Expression studies, however, suggest that the normal function of this gene may be in spermatogenesis and in the development of the central nervous system[3–5]. Genes sharing sequence similarity with *int-1* have been found throughout the animal kingdom. For example, *int-1* has 54% amino-acid identity to the *Drosophila* segment polarity gene *wingless* (*wg*)[6]. Both the *int-1* and *wg* gene products seem to be secreted proteins, presumably involved in cell–cell signalling[7–11]. We have now explored the function of *int-1* in the mouse by disrupting one of the two *int-1* alleles in mouse embryo-derived stem cells using positive–negative selection[12]. This cell line was used to generate a chimaeric mouse that transmitted the mutant allele to its progeny[13–16]. Mice heterozygous for the *int-1* null mutation are normal and fertile, whereas mice homozygous for the mutation may exhibit a range of phenotypes from death before birth to survival with severe ataxia. The latter pathology in mice and humans is often associated with defects in the cerebellum. Examination of *int-1*$^-$/*int-1*$^-$ mice at several stages of embryogenesis revealed severe abnormalities in the development of the mesencephalon and metencephalon indicating a prominent role for the *int-1* protein is in the induction of the mesencephalon and cerebellum.

Gene targeting has been used to disrupt numerous genes in mouse embryo-derived stem (ES) cells[12,17–28] and in several cases, germ-line transmission of the mutated gene has been reported[25–28]. The targeting vector we used to mutate *int-1*, pINT-1-N/TK, is shown in Fig. 1*a*. It contains 13 kilobases (kb) of mouse genomic DNA surrounding the *int-1* structural gene, which is interrupted in exon 2 by a 1-kb fragment containing the neomycin resistance (*neo*^{r}) gene, and flanked by copies of the thymidine kinase (*TK*) gene from herpes simplex virus.

* To whom correspondence should be addressed.

TABLE 1 Phenotype of *int-1*$^-$/*int-1*$^-$ mice

(*a*) Mortality of *int-1*$^-$/*int-1*$^-$ mice

No. litters	No. pups	No. *int-1*$^-$/*int-1*$^-$	Day of death of *int-1*$^-$/*int-1*$^-$ pups 0–0.5	0.5–1.5	>30
5	42	10	6	3	1

(*b*) Genotype and phenotype of embryos

Days p.c.	Genotype	No. individuals	Brain morphology
14.5	+/+	3	Normal
	+/−	3	Normal
	−/−	2	Underdeveloped
17.5	+/+	7	Normal
	+/−	7	Normal
	−/−	4	Underdeveloped

Mice heterozygous at *int-1* were mated. (*a*) Mortality of live births: Five pregnancies proceeded to term and the nests examined at daily intervals. Dead offspring were removed and their DNA examined as described in the legend to Fig. 2. At day 30, DNA was extracted from tails of all living offspring and analysed by the same method. (*b*) Genotype and phenotype of embryos. Embryos were surgically removed from pregnant mothers at the times indicated and immersed in Bouin reagent. Yolk sacs were genotyped as described in Fig. 2. After 2 days in fixative, the embryonic brains were surgically removed, examined under a dissecting microscope and qualitatively compared. The 14.5-day embryos were from a single mother, the 17.5 embryos represent the sum of two pregnancies

The *neo*^{r} gene serves both to disrupt the *int-1* protein reading frame and to provide a positive selectable marker, resistance to growth in G418, for the presence of the *int-1* mutation. The *TK* genes, lying outside *int-1* homology, function in the presence of the antiviral agent gancyclovir (GANC), as negative selectable markers that allow enrichment for cells in which homologous recombination has occurred[12].

ES cells were transformed by electroporation with the vector, pINT-1-N/TK and then grown in the presence of G418 and GANC. DNA was extracted from those colonies resistant to both drugs and analysed by Southern transfer for an insertion mutation at *int-1*. Of 5×10^8 cells surviving electroporation, 5×10^6 gave rise to G418^r colonies and 400 were resistant to both G418 and GANC. One of the G418^r-GANC^r colonies, cell-line 54, proved to contain a targeted disruption in one of the two *int-1* genes. The targeted disruption frequency for *int-1* was considerably lower than previously reported for *hprt* (ref. 17), *int-2* (ref. 12), *en-2* (ref. 20), c-*abl* (ref. 25), *IGF-II* (ref. 27) and β_2-microglobulin[22,24], which may reflect inherent differences of the loci.

The demonstration of gene targeting in cell-line 54 is illustrated in Fig. 1*b*. DNAs from the parental ES cell line (CCl.2)[13] and cell-line 54 were digested with *Sac*I and analysed by Southern blotting using a hybridization probe (probe A) that contained sequences outside those found on the targeting vector. In the parental line, this probe detected a 4-kb fragment of DNA. In the mutant cell line, an additional *int-1* band of 5 kb, was evident, consistent with the insertion of the 1-kb *neo*^{r} gene into *int-1*. This interpretation was verified by digestion of this DNA with two additional restriction enzymes and probing with *neo* sequences (data not shown). The same DNAs were digested with *Bgl*II and *Xho*I and analysed with a probe (probe B) contained within the vector sequences. In addition to the wild-type allele, DNA from cell-line 54 also revealed two fragments derived from the mutant, *int-1*$^-$ allele. One of these, of 4 kb, is that predicted for the *neo*^{r} insertion; the other, of 4.3 kb, is from a tandem duplication (described in the legend to Fig. 1) and subsequent insertion of vector sequences at the target site. This duplication–insertion configuration was verified by six independent enzyme digests (data not shown) and is similar to targeting events described by others[29,30].

Chimaeric mice were generated by microinjecting the male ES cell-line 54—originally derived from a 129 Sv agouti mouse—into blastocysts from C57Bl/6 nonagouti mice. One male chimaera, when mated to a C57Bl/6 female sired pure agouti offspring indicating that his germ line contained sperm derived from ES cell-line 54. DNA prepared from tail biopsies taken from the chimaera and two of his agouti offspring was analysed by Southern transfer as shown in Fig. 2*a*. DNA from the parental ES cell line and cell-line 54 serve as controls for the *int-1*$^+$/*int-1*$^+$ and *int-1*$^-$/*int-1*$^+$ genotypes, respectively. As expected, the chimaeric father contained *int-1*$^-$ sequences, but not in stoichiometric amounts, a reflection of the degree of chimaerism in the tail. Both of his offspring, however, show the same *int-1*$^-$/*int-1*$^+$ genotype stoichiometry seen in the original mutant cell line.

The heterozygous offspring were bred with C57Bl/6 mice to establish a colony of mice heterozygous for the *int-1*$^-$ mutation. Sibling heterozygotes were mated and the pregnancies allowed to proceed to term. All offspring were genotyped at the *int-1* locus by analysing tail DNA by Southern blotting. Table 1 summarizes the fate of ten *int-1*$^-$/*int-1*$^-$ offspring (from five litters): six were dead within 0.5 days of birth; three survived 0.5 days but died before day 1.5 and one survived to adulthood. Variation in survival may reflect variation in the penetrance of the *int-1* mutation or variability in the nurturing by the mother; female mice will often separate malfunctioning offspring from the rest of the litter. But in our experiments, one out of six homozygous *int-1*$^-$ mice (two litters) examined before birth at 17.5 days p.c. died *in utero*.

The *int-1*$^-$/*int-1*$^-$ mouse that survived to adulthood was most informative regarding *int-1* function. She exhibited severe ataxia. When moving, she pivoted both clockwise and counterclockwise around her rear legs. This abnormal pattern of movement was not due to muscle wastage or defects in local motor neuron circuitry as she could jump more than 30-cm vertically. Relative to heterozygous siblings, she responded normally to stimuli of light, sound, smell and touch.

The presence of this behavioural phenotype in the *int-1*$^-$ homozygote (that is, the loss of balance and coordinated movement) suggested a defect in the cerebellum and prompted us to examine the central nervous system (CNS) in embryos produced from heterozygous matings. Embryos were removed from pregnant females at 11.5, 14.5 and 17.5 days p.c. The DNA was extracted from the yolk sacs and analysed by Southern transfer to determine the *int-1* genotype; the embryos were then fixed

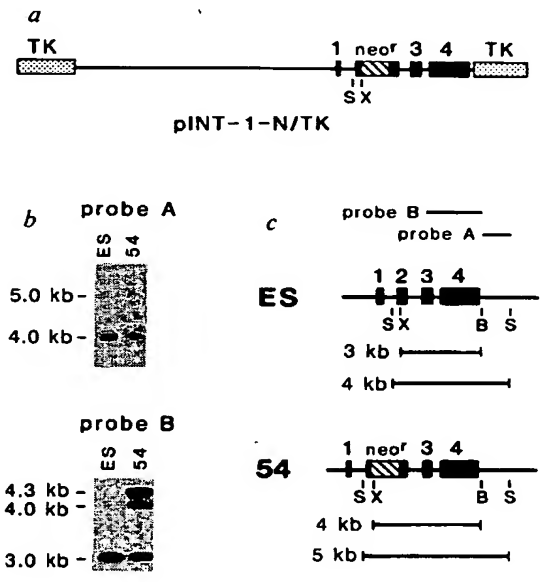

FIG. 1 *a*, The targeting vector, pINT-1-N/TK, consists of 13.5 kb of mouse genomic sequences, containing the *int-1* gene interrupted at the *Xho*I site in exon 2 (ref. 2) with the *neo*^{r} gene from pMCI-Neo (ref. 17). The *int-1-neo*^{r} sequences are flanked by copies of the *HSV-TK* gene from pMCI-TK (ref. 12). Narrow lines, introns; black boxes, exons; hatched boxes, *neo*^{r}; stippled boxes, *HSV-TK*. The vector was linearized by digestion with *Sal*I, and introduced into ES cell line CC1.2 by electroporation. Aliquots of cells were subjected to three growth conditions: non-selective medium to assess viability (50% of the starting cells survived electroporation); G418 medium to assay the fraction of cells stably transformed by the vector; and G418 plus GANC medium to enrich for transformants containing a *neo*^{r} insertion at one of the *int-1* loci. DNA from cells surviving G418-GANC selection were subjected to Southern transfer analysis as shown in *b*. Note: The presence of flanking *TK* sequences was included to add an additional enrichment to the positive–negative selection protocol. Previous data suggested that a large fraction of non-targeted, yet GANC^r, cells transformed with vector containing a single *TK* survived because of transfection-induced alterations of the *TK* gene[12]. The presence of the second copy of the *TK* sequences does seem to enhance the enrichment factor from the 10^3 seen previously, to 10^4 (that is, $5\times10^6/4\times10^2$), seen in Table 1. We have shown that blocking none, one, or both ends of a targeting vector has no detectable effect on the frequency of homologous recombination at the *hprt* locus (K.R.T. and M.R.C., unpublished observations). *b*, Identification of an *int-1*$^+$/*int-1*$^-$ cell line. ES, DNA from cell line CC1.2, 54, DNA from the G418^r, GANC^r cell line transfected with pINT-1-N/TK. Sizes of the bands are indicated (kb). DNAs hybridized to probe A were digested with *Sac*I; those to probe B with *Bgl*II and *Xho*I. The *int-1*$^+$ allele gives a stronger signal than the *int-1*$^-$ allele because of wild-type sequences in the feeder cells used to propagate the ES cells. *c*, A schematic representation of the Southern transfer data. ES is a map of the wild-type *int-1*$^+$ locus; 54 is a map of the *int-1*$^-$ allele containing a *neo*^{r} insertion in exon 2. Beneath each gene are shown the positions of diagnostic restriction endonuclease cleavage sites, and the length of the digestion products. Positions of the probes are indicated above the maps. Probe A (DNA sequence not present in the targeting vector) is a 1-kb *Bgl*II–*Hind*III fragment 3′ of the *int-1* gene (gift of R. Nusse); Probe B is a 2-kb *Cla*I–*Bam*HI fragment within the *int-1* gene. B, *Bgl*II; S, *Sac*I; X, *Xho*I. When DNA from cell line 54 is hybridized with probe B, which consists of sequences from within the vector pINT-1-N/TK, an unexpected fragment 4.3 kb in length is seen. This fragment represents additional copies of the vector sequences that have integrated in a tandem array 5′ to those sequences depicted. Such a configuration is most likely the result of the head-to-tail concatamerization of the vector before its recombination with the target locus. The 4.3-kb fragment extends from the *Xho*I site in exon 2 to a *Bgl*II site in the targeting vector and is predicted from the map of the vector. Digestions of DNA from cell-line 54 with six additional restriction endonucleases and hybridization with *neo*^{r} probes verify this configuration. The above analysis also showed that DNA sequences both 5′ and 3′ to the *int-1* locus were not altered, demonstrating that the targeted mutation was limited to the *int-1* gene.

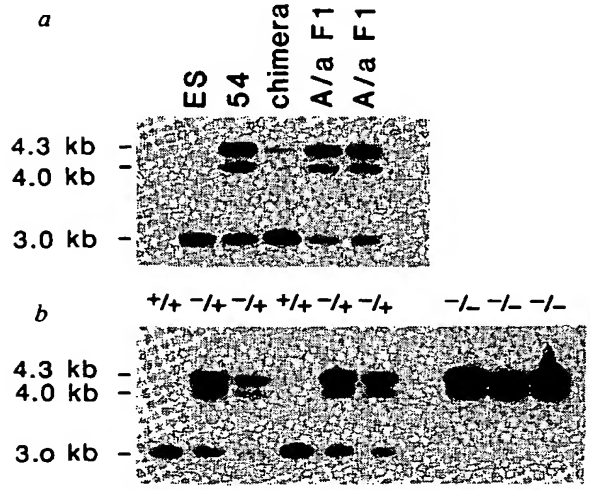

FIG. 2 Transmission of the *int-1*$^-$ genotype. *a*, Cell lines and founding animals. ES cell line 54 was microinjected into 4.5 day C57Bl/6 preimplantation embryos, surgically transferred into the uterus of pseudopregnant mice and allowed to come to term. Two resulting male chimaeras were test bred with C57Bl/6 females for transmission of agouti offspring. One of these males proved to be a germ-line chimaera. DNA was extracted from cell lines (ES and 54) or from tail biopsies, digested with *Xho*I and *Bgl*II, and analysed with probe B as described in the legend to Fig. 1. ES, the parental cell line CC1.2; 54, the *int-1*$^+$/*int-1*$^-$ cell line carrying the targeted mutation in *int-1*. Chimaera designates the founding chimaeric male; A/a and A/a are his agouti offspring produced following mating with a C57Bl/6 female. *b*, Transmission to embryos. Heterozygous offspring from A/a and A/a shown in *a* were mated. Following 17.5 days gestation, the embryos were removed from the mother. DNA was extracted from the yolk sac surrounding each individual embryo and analysed by Southern transfer as described in Fig. 1. The genotype at *int-1* is indicated above each lane: +, wild type; −, *neo*^{r} insertion in exon 2.

and dissected. DNA analyses of nine embryos from one pregnancy is illustrated in Fig. 2*b* and all three expected genotypes were clearly present. The results of visual analyses of the fetal brains are summarized in Table 1(*b*). After 11.5 days of gestation, morphological differences between heterozygous and homozygous *int-1*$^-$ mice were not readily apparent. But by 14.5 days, malformations in the mesencephalon and metencephalon were apparent. At 17.5 days, this malformation was translated into mild midbrain hydrocephaly. This malformation was 100% concordant with the homozygous *int-1*$^-$ genotype: 6/6 embryos of *int-1*$^-$/*int-1*$^-$ genotype exhibited this phenotype, whereas 20/20 *int-1*$^+$/*int-1*$^+$ and *int-1*$^+$/*int-1*$^-$ embryos showed normal brain development. Figure 3*a* and *b* compares dorsal views of brains from *int-1*$^-$/*int-1*$^+$ and *int-1*$^-$/*int-1*$^-$ embryos at 17.5 days of gestation. It is apparent from macroscopic examination alone, that the mesencephalon and metencephalon are highly defective. This is corroborated by examination of sagittal and parasagittal sections of the same brains (Fig. 3*c*, *d*). In the *int-1*$^-$ homozygote, the cerebellum and a large portion of the mesencephalon, as indicated by the arrows, are not visible. As a reference point, note that the posterior choroid plexus (pcp) is present in both brains. The embryos used for the above analysis, from the same mating, showed normal embryonic leg and head movement and touch response. The telencephalon as judged from examination of both parasagittal and coronal sections, appeared to be normal. However, in the *int-1*$^-$ homozygous mouse, the frontal lobes of the brain do seem to extend more caudally relative to the heterozygous mate, perhaps a result of expansion into regions normally occupied by the missing parts of the midbrain.

The *int-1*$^-$/*int-1*$^-$ mouse that survived until adulthood exhibited hydrocephally in the caudal region of the cerebral hemispheres as well as in the midbrain. Examination of sagittal and parasagittal sections of this *int-1*$^-$/*int-1*$^-$ brain corroborated the presence of the hydrocephally but also unexpectedly showed that the posterior portion of the cerebellum was present (Fig. 3*e*, *f*). In this context, it is interesting that Wilkinson *et al.*[5] did not observe *int-1* messenger RNA in the 10.5-day rostral hindbrain. Furthermore, LeDouarin and co-workers have recently provided evidence that in the chick, the anterior portion of the cerebellum may be derived from the mesencephalon, whereas the posterior portion comes from the metencephalon[31]. If this is also true for the mouse, then the phenotypic influence of the *int-1* mutation in this mouse may have respected the mesencephalon-metencephalon boundary.

In summary, heterozygous *int-1*$^-$ mice seem normal. A prominent effect of disrupting both *int-1* alleles is a major defect in the development of the midbrain and cerebellum. In fact, it seems that *int-1* protein is required in the induction of a large portion of the mesencephalon and of the cerebellum as in its absence these structures are not formed normally. Further, the *int-1* homozygote that survived to adulthood displayed the classical, although a more extreme, form of symptomatology attributed to human and mouse cerebellar defects (that is, severe ataxia).

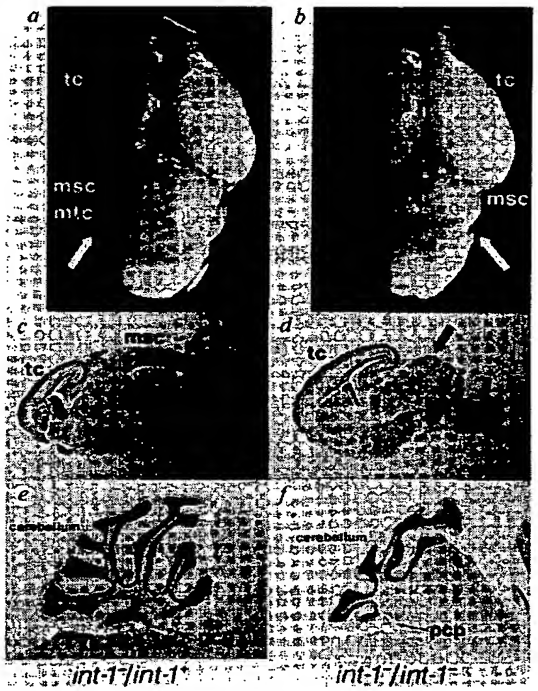

FIG. 3 Comparison of brains from heterozygous and homozygous, *int-1*$^-$ mice. *a*, and *b*, 17.5 day embryos were fixed in Bouin's reagent (Sigma). The yolk sacs were removed for DNA analysis as described in Table 1. Following two days in fixative, the brains were dissected, rinsed in PBS and photographed at ×6 magnification. The field of view is 5 × 10 mm. Arrows indicate the cerebellar region absent in the homozygote. *c* and *d*, The brains shown in *a* and *b* were embedded in paraffin, sectioned (10 μm), and stained by haematoxylin and eosin (H and E) regressive staining. The field of view is 6 × 4 mm. Arrows indicate mesencephalic tissue absent in the homozygote. *e* and *f*, Brains were dissected from adult (5 week) mice, fixed in PLP, embedded in paraffin, sectioned (8 μm) stained with H and E. The field of view is 6 × 4 mm. tc, telencephalon; msc, mesencephalon; mtc, metencephalon; pcp, posterior choroid plexus.

In the 17.5-day embryo, cellular structures corresponding to the cerebellum are not observed. But in the mouse that survived to adulthood, the posterior portion of the cerebellum was present. An intriguing hypothesis to explain this difference is that the dependency on the inductive influence of *int-1* exhibits a rostral-caudal gradient beginning in the mesencephalon and spreading to the metencephalon. This could produce differences in the penetrance of the *int-1*$^-$ mutation such that some mice lack only the anterior portion of the cerebellum, whereas others are missing the entire cerebellum.

The *int-1* gene is expressed during the ontogeny of the CNS along the dorsal midline of the developing neural tube from the midbrain to the tail[5]. From analysis of sagittal and transverse sections, in either embryos or in the *int-1*$^-$ survivor, we have not observed morphological defects in the spinal cord. This may indicate that either *int-1* expression in this region of the developing CNS is spurious or that another gene, perhaps another member of the *int-1* family, can substitute for *int-1* function in the development of the spinal cord. □

Received 20 July; accepted 6 August 1990.

1. Nusse, R. & Varmus, H. E. *Cell* **31**, 99-109 (1982).
2. van Ooyen, A. & Nusse, R. *Cell* **39**, 233-240 (1984).
3. Jakobovits, A., Shackleford, G. M., Varmus, H. E. & Martin, G. R. *Proc. natn. Acad. Sci. U.S.A.* **83**, 7806-7810 (1986).
4. Shackleford, G. M. & Varmus, H. E. *Cell* **50**, 89-95 (1987).
5. Wilkinson, D. G., Bailes, J. A. & McMahon, A. P. *Cell* **50**, 79-88 (1987).
6. Rijsewijk, F. *et al. Cell* **50**, 649-657 (1987).
7. Morata, G. & Lawrence, P. A. *Devl Biol.* **56**, 227-240 (1977).
8. Baker, N. E. *EMBO J.* **6**, 1765-1770 (1987).
9. Papkoff, J., Brown, A. M. C. & Varmus, H. E. *Molec. cell. Biol.* **7**, 3978-3984 (1987).
10. Bradley, R. S. & Brown, A. M. *EMBO J.* **9**, 1569-1575 (1990).
11. Papkoff, J. & Schryver, B. *Molec. cell. Biol.* **10**, 2723-2730 (1990).
12. Mansour, S. L., Thomas, K. R. & Capecchi, M. R. *Nature* **336**, 348-352 (1988).
13. Bradley, A., Evans, M., Kaufman, M. H. & Robertson, E. *Nature* **309**, 255-256 (1984).
14. Capecchi, M. R. *Trends Genet.* **5**, 70-76 (1989).
15. Capecchi, M. R. *Science* **244**, 1288-1292 (1989).
16. Rossant, J. & Joyner, A. *Trends Genet.* **5**, 277-283 (1989).
17. Thomas, K. R. & Capecchi, M. R. *Cell* **51**, 503-512 (1987).
18. Doetschman, T., Maeda, N. & Smithies, O. *Proc. natn. Acad. Sci. U.S.A.* **85**, 8583-8587 (1988).
19. Zimmer, A. & Gruss, P. *Nature* **338**, 150-153 (1989).
20. Joyner, A. L., Skarnes, W. C. & Rossant, J. *Nature* **338**, 153-156 (1989).
21. Johnson, R. S. *et al. Science* **245**, 1234-1236 (1989).
22. Koller, B. H. & Smithies, O. *Proc. natn. Acad. Sci. U.S.A.* **86**, 8932-8935 (1989).
23. Mansour, S. L., Thomas, K. R., Deng, C. & Capecchi, M. R. *Proc. natn. Acad. Sci. U.S.A.* (in the press).
24. Zijlstra, M., Li, E., Sajjadi, F., Subramani, S. & Jaenisch, R. *Nature* **342**, 435-438 (1989).
25. Schwartzberg, P. L., Goff, S. P. & Robertson, E. J. *Science* **246**, 799-803 (1989).
26. Zijlstra, M. *et al. Nature* **344**, 742-746 (1990).
27. DeChiara, T. M., Efstratiadis, A. & Robertson, E. J. *Nature* **345**, 78-80 (1990).
28. Koller, B. H., Marrack, P., Kappler, J. W. & Smithies, O. *Science* **248**, 1227-1230 (1990).
29. Fell, H. P., Yarnold, S., Hellstrom, I., Hellstrom, K. E. & Folger, K. R. *Proc. natn. Acad. Sci. U.S.A.* **86**, 8507-8511 (1989).
30. Schwartzberg, P. L., Robertson, E. J. & Goff, S. P. *Proc. natn. Acad. Sci. U.S.A.* **87**, 3210-3214 (1990).
31. Hallonet, M. R., Teillet, M. & LeDouarin, N. M. *Development* **108**, 19-31 (1990).

ACKNOWLEDGEMENTS: We thank S. Tamowski, C. Lenz, M. Allen and E. Nakashima for technical assistance, T. Musci and R. Mullen for assistance and advice on histology, R. Nusse for providing the *int-1* flanking probe, O. Gard and F. Brown for help with photography.

'Formins': proteins deduced from the alternative transcripts of the *limb deformity* gene

Richard P. Woychik*, Richard L. Maas*, Rolf Zeller*, Thomas F. Vogt & Philip Leder

Department of Genetics, Harvard Medical School, and Howard Hughes Medical Institute, 25 Shattuck Street, Boston, Massachusetts 02115, USA

VERTEBRATE limb formation is an evolutionarily conserved process programmed by an array of morphogenetic genes[1-5]. As a result of transgene insertion, we previously identified a mutation at the mouse limb deformity (*ld*) locus that disrupts embryonic pattern formation, resulting in a reduction and fusion of the distal bones and digits of all limbs as well as variable incidence of renal aplasia[2,6-9]. We have now characterized the *ld* locus at the molecular level. It contains evolutionarily conserved coding sequences that are transcribed in adult and embryonic tissues as a complex group of low abundance messenger RNAs created by alternative splicing and differential polyadenylation. The association of these transcripts with the gene responsible for the mutant phenotype was established by demonstrating that they are disrupted in two independently arising *ld* alleles[8]. We have now deduced the structure of several novel proteins (termed formins) from the long open reading frames encoded by the various *ld* transcripts. The observation of these different RNA transcripts in different tissues suggests that the formins play a part in the formation of several organ systems.

A map of both the mutant and wild-type loci is shown in Fig. 1*a*. Insertion of the transgene into the (*ld*) locus was accompanied by deletion of about 1.5 kilobases (kb) of endogenous genomic DNA[6]. No other rearrangements were observed. We first identified potential exons along the genomic DNA by searching for evolutionarily conserved regions. Two of these appeared as likely coding exons because, when sequenced, they revealed short open reading frames flanked by splice acceptor-donor sequences (A and B in Fig. 1*a*). Cross-hybridizing regions were cloned from human and chicken genomic libraries and examined for sequence homology. The nucleotide sequences of regions A and B are 80-90% conserved between humans and mice. For example, the extent of sequence conservation of one putative exon (Fig. 1*a*, region B) is shown by comparing the homology regions of the mouse, human and chicken genomes (Fig. 1*b*).

Complementary DNA libraries prepared from RNA isolated from adult kidney and testis (two organs in which transcripts were most abundant) yielded overlapping cDNA clones that were identified using a genomic DNA probe containing the evolutionarily conserved exon B (shown in Fig. 1*a*, *b*). Sequence analysis of these cDNAs, illustrated by ten representative cDNA clones (Fig. 2), demonstrates a complex pattern of mRNA synthesis (see also Fig. 3). These cDNAs reveal differential use of polyA addition sites separated by several kilobases as well as alternative splicing of internal (see clones 2, 3, 4, 5, 7 and 9, Fig. 2) and 5′ exons (see clone 1, Fig. 2). Long, but variably composed open reading frames (ORFs) (see below) were deduced from nucleotide sequence analysis.

The complexity of the RNA products of the *ld* locus is reflected by the various transcripts observed in analyses of RNA from both embryonic and adult tissues (Fig. 3). A transcript important in morphogenesis of limb and kidney should be present before or at the time of the morphological observation of the mutant phenotype. Expression of the *ld* gene as assayed by RNase protection occurs in primitive-streak embryos (gestational day seven) before limb development[9]. To examine the pattern of RNA transcripts in the embryo, RNA was isolated from gestational day 9-12 embryos and analysed as shown in Fig. 3*a*. Three main classes of mRNAs (~13, 7 and 3 kb) are detected in all parts of the embyro (Fig. 3*a*) including the limb buds. The size differences observed between these transcripts result from differential utilization of the three sets of poly(A)

* Present addresses: Biology Division, Oak Ridge National Laboratories, PO Box 2009, Oak Ridge, Tennessee 37831, USA (R.P.W.); Department of Medicine, Brigham & Women's Hospital, Howard Hughes Medical Institute, Boston, Massachusetts 02115, USA (R.L.M.), and EMBL, Postfach 10.2209, Meyerhofstr. 1, D-6900 Heidelberg, FRG (R.Z.).